

# Tex-ViT: A Generalizable, Robust, Texture-based dual-branch cross-attention deepfake detector

Deepak Dagar<sup>1</sup>, Dinesh Kumar Vishwakarma<sup>2,\*</sup>

Biometric Research Laboratory, Department of Information Technology, Delhi Technological University,  
Bawana Road, Delhi-110042, India

[deepakdagargate@gmail.com](mailto:deepakdagargate@gmail.com)<sup>1</sup>, [dvishwakarma@gmail.com](mailto:dvishwakarma@gmail.com)<sup>2,\*</sup>

## Abstract

Deepfakes, which employ Generative Adversarial Networks (GANs) to produce highly realistic facial modification, are widely regarded as the prevailing method. Traditional Convolutional Neural Networks (CNNs) have been able to identify bogus media, but they struggle to perform well on different datasets and are vulnerable to adversarial attacks due to their lack of robustness. Vision transformers have demonstrated potential in the realm of image classification problems, but they require enough training data. Motivated by these limitations, this publication introduces Tex-ViT (Texture-Vision Transformer), which enhances CNN features by combining ResNet (Residual Networks) with a vision transformer. The model combines traditional ResNet features with a texture module that operates in parallel on sections of ResNet before each down-sampling operation. The texture module then serves as an input to the dual branch of the cross-attention vision transformer. It specifically focuses on improving the global texture module, which extracts feature map correlation. Empirical analysis reveals that fake images exhibit smooth textures that do not remain consistent over long distances in manipulations. Experiments were performed on different categories of FaceForensics++ (FF++), such as Deepfakes (DF), Face2Face (f2f), Faceswap (FS), and Neural Texture (NT), together with other types of GAN datasets in cross-domain scenarios. Furthermore, experiments also conducted on FF++, DFDCPreview, and Celeb-DF dataset underwent several post-processing situations, such as blurring, compression, and noise. The model surpassed the most advanced models in terms of generalization, achieving a 98% accuracy in cross-domain scenarios. This demonstrates its ability to learn the shared distinguishing textural characteristics in the manipulated samples. These experiments provide evidence that the proposed model is capable of being applied to various situations and is resistant to many post-processing procedures.

**Keywords:** Deepfake detector, Texture, Gram matrices, Generalization, Robustness.

## 1 Introduction

With the advancements in technology, especially GANs, it is possible to generate highly realistic content that can easily deceive the naked eye. Deepfake is a current state of the art of visual and audio manipulation. Deepfake is a technology where highly astonishing, realistic, and believable content is created using deep learning technology (Figure 1). Visual deepfakes can be classified into five categories: lip sync, attribute manipulation, full-image synthesis, body re-enactment, and face ap [1]. The application of the deepfake has benefitted the education and entertainment industry in various ways. Still, its malicious aspects have threatened the individual's reputation, creating chaos in society and threatening the nation's peace [1].



Figure 1: Example of Deepfake [2]

Various approaches have been devised to counter the anti-social elements' malicious intent. These approaches use various clues like GAN-based artifacts [3] [4], visual artifacts [5] [6], biological signals [7] [8], temporal inconsistency between frames [9] [10], audio-visual inconsistency [11] [12], while other let the Deep Neural Networks models [13] [14] learn the intrinsic features of the distribution. The majority of these models exhibit strong performance when used inside the same domain as the training and testing data, but they struggle when applied to different domains. Also, these methods result in a decline in performance in real-world scenarios where visual data can undergo compression, experience the addition of noise, and encounter unanticipated data blur [15]. Nevertheless, certain approaches have partially addressed these issues [16] [17] [18]. More work needs to be done to bridge this gap. Furthermore, CNN algorithms with narrower receptive fields [25] may fail to capture the long-term correlation of features. Long-range feature modeling necessitates the incorporation of an extra module within the CNN model to account for global texture at various semantic levels.

In the cross-domain context, a model needs to identify features that are consistent across the false data sets. Texture is an example of such a feature. To address the above limitations, a texture-based multi-scale cross-attention transformer has been developed. The model posits that counterfeit images exhibit smooth surfaces, and the overall texture remains consistent across the synthetic data samples. The model combines traditional ResNet features with a texture module that operates in parallel on sections of ResNet before each down-sampling operation. The texture module then serves as an input to the dual branch of the cross-attention vision transformer. The motivation for integrating CNN with vision transformer stems from the limitations of CNNs in capturing global properties that exhibit variations over greater distances, due to their inherent inductive biases such as equivariance, translation, and locality of reference. Nevertheless, vision transformers, equipped with inherent attention mechanisms, are capable of precisely capturing such global aspects. The paper's contribution can be summarized as follows:

- An empirical analysis from human and CNN's perspective states that texture statistics play a vital role in the discrimination of fake media. Also, the analysis found that longer-range texture correlation is not preserved in the simulated images.

- Experimentation was done on the FF++ and GAN images dataset categories to show the generalizable abilities of the cross-dataset distribution. The model easily outperforms the other state-of-the-art models and confirms that texture statistics play a vital role in detecting fake manipulated samples.
- Experimentation was done on the Celeb-DF, FF++, and DFDCPreview with different post-processing operations like blurring; the addition of noise and compression shows that the model can beat the scores of others easily, showing robustness in various scenarios.
- Ablation studies were performed on each component of the model to demonstrate the component's effectiveness and the efficacy of their combination and prove that texture with a cross-attention mechanism is a powerful feature.
- Complexity computational analysis is performed against various state-of-the-art computer vision and deepfake detection models to exhibit that the proposed model is light-weight with 43 million parameters and performs better than the former models in diverse scenarios.

The remaining sections of this manuscript are organized as follows: section 2 describes the related work done in this field, including deepfake generation and detection methods. Section 3 discusses the empirical analysis to demonstrate the effectiveness of texture as a feature for classification. Section 4 presents the proposed model and a description of its various components. Section 5 explains the experimentation setup, data pre-processing and data augmentation techniques, experimentation on cross-domain settings on the FF++ and various GAN images, and the in-domain setting for various post-processing operations. Section 7 presents the ablation studies of different components to discuss their importance in feature extraction. Section 8 presents the visualization results for each dataset image.

## 2 Related Work

The significant research contributions for deepfake detection are discussed in this section.

### 2.1 Deepfake Image Synthesis

The advancement of GAN technology has taken significant strides in generating realistic images since its inception by Goodfellow [19]. Deepfake Image synthesis can be classified as identity Swap, Attribute Manipulation, and Entire face synthesis [1]. **An identity swap transfers** identity from the source to the target. Face-swap [20] and Fake-App [21] use auto-encoder and decoder for identity swap. Their standard methodology for FS relies on a dual auto-encoder and decoder framework [1]. The initial and widely recognized instance of an identity swap is FaceSwap [20], which was utilized in the creation of the FaceForensics++ dataset [22]. The recent face-swap techniques use GANs owing to their ability to generate highly realistic faces[1]. In recent years the face swap technology has become more sophisticated, owing to the sophistication of the deep learning approaches [2], [3], [4], [5], [6]. StyleSwap[7] The style-based GAN employs an architecture that effectively incorporates the needed information from both branches. Additionally, a layer masking branch is included to enhance the blending information further. FSGANv2[8] employs the technique of reenacting delaunay triangulation and barycentric coordinates, followed by building a face-blending network to achieve a smoothing effect. Model[9] also uses a 3D aware face swapping technique for swapping faces in 3D, which produces high-quality and visually consistent swapped faces from single-view source and target images. It exploits the robust geometric and textural characteristics of 3D human faces, whereby the 2D faces are mapped onto the underlying space

of a 3D generative model by separating the identification and attribute characteristics in the latent space. Other models also incorporate the 3D-aware techniques with a mask diffusion process; Zhao et al.[10] uses a mid-point estimation method that consists of a two-point segmentation method, which allows for the incorporation of identity constraints to produce high-quality faces. Faceshifter [23] is another method that generates highly realistic images using an encoder and generator in a self-supervised manner. **Attribute Manipulation** is another image manipulation category where various facial attributes like expressions, eyes, age, and mustache are manipulated in an image. Such methods generally employ ED or a combination of ED with GANs with a conditioned attribute[11], [12], [13], [14], [15]. StarGAN [24] and STGAN [25] are typical examples of it over the years. Yang et al. [14] provide a solution based on GAN utilizing dilated convolutions to adjust the receptive fields of shallow layers in StyleGAN. This approach enables the expansion of fixed-size tiny features at shallow layers into larger ones that can adapt to varying resolutions, hence enhancing their ability to describe unaligned faces accurately. Facial attributes generally use the disentanglement of attributes in the latent space, which allows manipulation to be carried out in the desired way. Liu et al. [13] alter the underlying code in the 'style space' and provide 'Style Intervention,' a streamlined optimization-based technique, to enhance the visual accuracy of manipulation outcomes. Huang et al.[11] introduce a new method called AdaTrans, which is an adaptive non-linear latent transformation for disentangled and conditional face editing. The approach breaks down the manipulation process into multiple smaller steps, wherein at each step, the direction and size are determined based on both the facial features and the hidden codes. Current works frequently fail to retain the domain-invariant component of the image, such as the identity of human faces. Liu et al.[12] introduce an implicit style function (ISF) as a method to efficiently do image-to-image translation across multiple modes and domains using pre-trained unconditional generators. The ISF modifies the latent representation of an underlying code so that the resulting image falls inside the intended visual range.

**Entire Image synthesis**, where the whole image is synthesized using powerful GANs. ProGAN[16] and StyleGAN[17] are the popular examples that have been proposed over the years. The authors have enhanced the architecture of StyleGAN2[18] by incorporating the normalization technique employed in the generator. In addition, they modified the progressive GAN method by imposing constraints on the mapping of the generator, ensuring a more controlled transformation from the latent code to images. In StyleGAN3[19], the authors observe the aliasing effect by considering all signals in the network as continuous and may deduce simple architectural modifications that are universally applicable and ensure that undesired information cannot infiltrate the hierarchical synthesis process. Many techniques struggle to strike a balance between the accuracy and diversity of produced samples. Diffusion-based models, such as ConPreDiff[20], have been employed for diffusion-based synthesis. This significant method focuses on preserving semantic connections between nearby pixels, resulting in the development of high-quality image synthesis. Another approach uses Latent diffusion models to generate high-resolution images. Podell et al. [20] created the SDXL, a system that integrates multiple novel conditioning techniques and is trained on different aspect ratios. In addition, they provide a refinement model that improves the visual quality of samples generated by SDXL using a post-hoc image-to-image technique. Various famous datasets have been proposed: Faceforensics, Faceforensics++, Celeb-DF, DFDC, and Deepforensics. These datasets use face manipulation techniques or a combination of several face manipulation techniques.

## 2.2 Deepfake detection

Since the advent of this technology, there have been very famous approaches that look for various clues/features for fake detection; after all these technological advancements in the respective fields, these methods do not generalize well on unseen samples. In other words, these methods fail to perform well on the cross-dataset, and they are not robust enough against various pre-processing operations like blurring, compression, and addition of noise. Different detection approaches have solved it to a certain extent. Khalid et al. [13] approach-based class detection approaches use a Variational Encoder, which is trained on real human face images, and other classes are considered anomalies, such as deepfakes. However, the method relies on the RMSE function to compute the reconstruction scores of the images. Their performance is unclear to the GAN-generated images; hence, the model is not generalizable. Li et al. [5] use face X-rays for a more general face forgery detection. The method assumes the existence of blending boundaries and decomposes the input image into integrating two or more sources. However, the method may fail for entirely synthetic images, and an adversary can develop an adversarial example that can bypass the detection mechanism and, hence, is not generalizable to different types of manipulations and robust against the various detection scenarios. Wang et al. [26] proposed a novel approach that is based on monitoring the neuron's behavior layer by layer, and such interaction patterns produce subtle artifacts for detection. Still, the algorithm's performance is far from satisfactory, and adversaries can develop adversarial examples that can evade the detection mechanism and, hence, are not robust enough. Other methods( [27] [28]) use co-occurrence matrices as input on the image pixels to compute the disparities along various spatial and spectral band channels and then pass through CNNs for fake face detection. However, the information included in the raw data is lost due to handcraft features.

Generalization for the deepfake detector has been a critical issue, and various researchers have addressed it [29] [30] [31] [32] [33] [34]. A generalizable detector can perform on the cross-datasets, enabling it to perform well on unseen datasets and the dataset that undergoes various adversarial operations like noise, blur, and compression of samples. Nadimpalli et al. [35] use a combination of reinforcement learning and supervised learning. The approach enables the choice of top-k augmentation for the test samples, which are averaged together for final classification. The model gives good results for generalizability, but their evaluation is limited to the Celeb-Df and FF++ datasets. The generalization model needs to uncover various common features among various kinds of manipulation. Researchers worked in that direction [36] [37]. Yu et al. [37] use a module's independently trained specific forgery feature extractor and U-Net architecture to examine the module's validity. However, the method assumes the presence of similar forgery traces, which could be hidden or concealed by the adversary. Atama et al. [38] use image noise residual domain to examine the training impact of spatial and spatial-temporal features to improve generalization, but their methodology is based on high-frequency information, which is insufficient for the data compression scenarios. Li et al. [39] designed a code detection tool that uses a codebook to capture the actual space distribution of authentic and forged images. The model performs well with various cross-dataset images and compressed images, but the model performance remains unclear to various other and wild datasets. The generalizability of the detector has been a critical challenge that needs to be explored for a detector to work in various adversarial scenarios

**Texture-based detection:** Texture of CNNs has grabbed much attention in the last few years. Various authors ( [40] [41] [18] [16] ) worked on the textures, as CNN models are intrinsically biased towards textures rather than shapes. Yang et al. [41] described a novel Multi-scale Texture Difference Model that provides a stationary description of texture difference by merging the information from pixels' gradient and intensity. The model performs well on

various distortions, but the performance is significantly reduced for unseen manipulation. Bonomi et al. [17] use Local Derivative Patterns on Three Orthogonal Planes (LDP-TOP) to explore the textural dynamics of the spatial and temporal dimensions. Though the model performs well on various manipulations of FF++, their performance remains questionable on various kinds of GAN images and heavy compression video samples. Yadav et al. [42] have a unique end-to-end architecture for facial manipulation detection that extracts discriminative "textural" (T) and "manipulation residuals" (MR) features from two branches in unequal proportions. The performance of the model remains questionable to unseen scenarios. Gao et al. [43] explore the similarities between various forged content in terms of texture characteristics and the presence of artifacts, based on that designed an ensemble which results in the model's generalization abilities. Method performance is not suitable for highly compressed scenarios. Yang et al. [40] approach discover the texture difference between fake and real images in image saliency, further enhanced by the guided filter with a saliency map. The method requires much data and must be trained again for unseen images. Liu et al. [16] leverage global image texture representations using gram matrices for robust fake image detection. Their performance remains unclear to other deepfake manipulations. These detection methods either lack generalization capabilities to unseen manipulation or are not powerful enough against various detection scenarios like the addition of noise, compression, and blurring. This paper proposed a texture-based approach that uses CNNs and multi-scale vision transformers to improve these limitations. The texture is computed using gram matrices on top of ResNet layers, which serve as input to ViT and conventional CNN features. The discriminative model shows its effectiveness in improving generalizability and robustness towards the manipulated artifacts.

### **3 Empirical Analysis**

The question confronting the research community is finding the common discriminative features for different fake images generated. Various researchers experimented in this regard [16] [18]; one of the critical findings of such experiments was that Texture statistics plays a vital role for various CNNs-based detectors like ResNet and successfully capture such texture differences for discrimination. This section presents the importance of texture as a feature for classification from different perspectives.

#### **3.1 Texture as a clue**

Texture refers to the appearance of the surface characterized by the shape, size, density, and proportionate arrangement of its elementary parts. In computer vision terminology, it is the repeated occurrence of the grey pixel level in the space [41]. An empirical analysis of the fake and real images is done to reveal the differences between textural characteristics. Texturized images are generated for accurate and fake images using a texturized generating algorithm, and it can be seen from Figure 2 that fake images lack texturized details compared to authentic images. This could be because forming fake tampered data samples usually involves three steps, i.e., pre-processing, face generation, and post-processing operation. Post-processing operations are generally done to hide such texture defects; as a result, counterfeit images tend to have a smoother surface and fewer texture characteristics [44]. Also, looking more closely at Figure 3, one finds that manipulated images come from smoother surfaces. Hence, the lack of a texturized surface would be a potential clue for fake image detection.



Figure 2: Real and fake Images are shown with their texturized images. Texturized images are generated from the images using the texture-based algorithm.



Figure 3: Fake images on a closer look showing that fake images tend to have smoother surfaces.

Human and Deep neural networks discern the images differently for their identification as real or fake. Humans usually identify artificial objects based on the shapes and colors of artifacts such as 'asymmetrical eyes,' 'uneven teeth,' 'irregular skin tone,' 'fairly smooth surfaces,' and more. [18]. Most of their identification is based on the shapes rather than the texture of the surface [45]. Reliance on these noticeable or high-level artifacts for identification misleads them easily, especially for entire-GAN image synthesis.

### 3.2 CNN Result Analysis

Many studies [46] [47] [48] have been done to capture the significance of various layers of CNNs and what each layer processes and learns. The widely accepted notion is that earlier layers of CNNs learn the low-level features like edges, lines, corners, etc., while the deeper ones learn the complex representations like faces, trees, etc. One of the more profound findings by the authors [1] is that CNN models are biased or inclined towards texture rather than shapes. In other words, CNN's models identify objects based on their surface rather than their shapes. Also, one of the exciting findings is that CNN's models cannot incorporate long-range information due to their small receptive fields [49]. Hence, CNNs need an additional module to integrate texture information into the module over much longer distances.

## 4 Proposed Model

The model comprises two components (Figure 4): texture Architecture and dual-branches cross-attention vision transformer. Texture architecture consists of two branches which serve as inputs to the parallel branches of the cross-attention vision transformer.

### 4.1 Texture Architecture:

Texture architecture constitutes resnet-18 architecture as a backbone, and the texture block is computed at the input and before every down-sampling operation incorporating global texture at various levels. The texture block consists of convolutional layers and gram matrices. Gram matrices are used to extract texture correlation, while convolution layers is then applied to enhance the representation, and pooling layers are used to align the computed features with the ResNet backbone features for the next level. The global Texture module is computed at multiple semantic levels before to each ResNet downsampling operation to model long-range texture features [16]. The main backbone of ResNet-18 learns the conventional features representation of the input images at various levels with a skip connection. It improves the gradient flow between the layers of the multi-scale features while the Texture block learns the global textures' semantic information at various scales.

*Gram matrices as Texture features:* Within a model, the texture is represented by the correlations among the features map responses in various model layers [50]. The Gram matrix quantifies the correlation between different feature map responses over different layers. These correlations, which are determined up to a constant factor, are represented by the gram matrices. Gram matrices  $G^l \in R^{N_l \times N_l}$  computes linear dependence between the layers:

$$G_{ij}^l = \sum_k F_{ik}^l F_{jk}^l \quad (i)$$

Equation (i) represents the gram matrix.  $G_{ij}^l$  which is the inner product between the  $i^{\text{th}}$  and  $j^{\text{th}}$  feature of layer  $l$ , where  $F^l$  represents the  $l^{\text{th}}$  feature map vectorized representation and  $F_{ik}^l$  represents the  $k^{\text{th}}$  activation of the  $i^{\text{th}}$  filter at position  $k$  in layer  $l$ . A texturized model, as defined, does not consider spatial information and is distinguished by the correlations among the feature maps. The texture is generated by computing gram matrices, which are calculated in the model prior to each downsampling operation of the ResNet. These matrices are then concatenated and used as input to the cross-attention mechanism of the vision transformer.

### 4.2 Dual branch Cross-Attention Vision Transformer

The vision transformer, free of inductive biases, is known for capturing long-range, global relationships between the pixels, courtesy of their self-attention mechanism and capacity for holding semantic information. The proposed architecture uses two parallel branches, and patches input into these branches are comparable in scale. The model takes the texture architecture's input, and then positional embedding is added into each patch, including the CLS token, to embed positional information into the model. Then, these tokens are passed through the stacked transformer encoder. Each transformer encoder contains a dual branch and is composed of Multi-headed self-attention(MSA) followed by the feed-forward Network(FFN) [51]. FFN includes two layers of the multi-layer perceptron, and the GELU non-linear layer is applied at the end of the first layers. Layer-Norm (LN) is used at the end of every block, with residual skip-connection applied after every block. The input to the  $x_0$  ViT and  $l^{\text{th}}$  processing of the transformer encoder can be written as:

$$x_0 = [x_{\text{class}} || x_{\text{patch}} E] + E_{\text{pos}} \quad E \in R^{P^2 \cdot C \times D}, E_{\text{pos}} \in R^{(N+1) \times D} \quad (ii)$$

$$z_l = z_{l-1} + MSA(LN(x_{l-1})), \quad l = 1 \dots L \quad (\text{iii})$$

$$x_l = z_l + FFN(LN(z_l)), \quad l = 1 \dots L \quad (\text{iv})$$

where  $x_{cls\_emb} \in \mathbb{R}^{1 \times C}$ ,  $x_{patch\_emb} \in \mathbb{R}^{N \times C}$  and  $x_{posemb} \in \mathbb{R}^{(N+1) \times C}$  are the cls, patch, and positional embedding tokens, respectively ( $C$  and  $N$  are the embedding's dimension and the number of the tokens). Afterward, the CLS token of one branch, which has learned the abstract information, acts as a token query to interact with the patch tokens of the other branch through an attention mechanism resulting in multi-scale features. Similarly, the CLS token interacts with the patch tokens of the other branch. The cross-attention mechanism is represented in the subsequent equations where  $x$  is the input to MSA (Multi-headed self-attention module):

$$x^1 = [x_{cls}^1 || x_{patch}^2] \quad x^1 \in \text{token } I^{st} \text{ branch}, \quad x^2 \in \text{tokens } II^{nd} \text{ branch} \quad (\text{v})$$

$$q = x_{cls}^1 W_q, \quad [k, v] = x^1 W_{kv} \quad W_q, W_{kv} \in \mathbb{R}^{D \times 3D_h} \quad (\text{vi})$$

$$A = \text{softmax} \left( \frac{qk^T}{\sqrt{D_h}} \right) \quad A \in \mathbb{R}^{N \times N} \quad (\text{vii})$$

$$SA(x^1) = Av \quad (\text{viii})$$

$$MSA(x^1) = [SA_1(x^1); SA_2(x^1); \dots; SA_k(x^1)] W_{msa} \quad W_{msa} \in \mathbb{R}^{k \cdot D_h \times D} \quad (\text{ix})$$

$$\hat{y}_{cls}^1 = x_{cls}^1 + MSA(LN([x_{cls}^1 || x_{patch}^2])) \quad (\text{x})$$

Where  $q$ ,  $k$ , and  $v$  are the query, key, and value, respectively,  $n+1$  is the number of patches,  $d$  is the model dimension,  $k$  is the number of heads, and  $D_h(d/k)$  is the head dimension.  $W_q$ ,  $W_{kv}$ , and  $W_{msa}$  are the learnable parameters for the query, key, value, and MSA, respectively. Following fusion with other branch tokens, the CLS token at the next transformer encoder engages with its patch tokens once more. Here, it imparts knowledge from the other branch to its patch tokens, enhancing each patch token's representation. Then, these tokens are passed through the Layer Norm to MLP (Multi-Layer Perceptron) for parameter learning:

$$\ddot{y}^1 = \hat{y}_{cls}^1 + x_{patch}^1 \quad (\text{xi})$$

$$\check{z} = MLP(LN(\ddot{y}^1)) \quad (\text{xii})$$

Finally, these classification tokens are concatenated for the final predictions.

---

### Algorithms 1: Tex-ViT for Deepfake classification

---

#### Parameter Initialisation:

- Input:  $I = \{I_1, I_2, \dots, I_n\}$  be the set of images, and  $L = \{0, 1\}$  be the set of labels, 0 being the real and 1 being the deepfake image
- $n$  is the size of the dataset
- Split  $I$  into three subsets for 70% training, 15% validation, and 15% testing.

#### 1: For 1 to 100 epochs, do

- 2: Input image  $I$  into ResNet for feature extraction.
- 3: Compute the texture using texture block before every down sampling operation in ResNet and keep concatenating them.
- 4: ResNet computed Fed conventional CNNs, and texture features were calculated at step 1 and step 2 into the dual branch of the vision transformer.
- 5: Split the features into patches (fixed sizes) and flatten them at each branch.

- 6: With these image patches flattened, create linear embeddings in lower dimensions.
  - 7: Include positional embeddings with CLS token.
  - 8: Feed the sequence into the transformer encoder at each branch.
  - 9: Create tokens by querying the CLS token of the I<sup>st</sup> branch with patch tokens of another branch and vice-versa.
  - 10: Concatenate the tokens of both branches for classification.
  - 11: Train the model end-to-end and update weights using the Adam optimizer.
  - 12: Evaluate the validation set and save the weights of the model that performs well.
  - 13: **end for**
  - 14: Load the weights of the model saved at step 11.
  - 15: Evaluate the performance on the test set
-

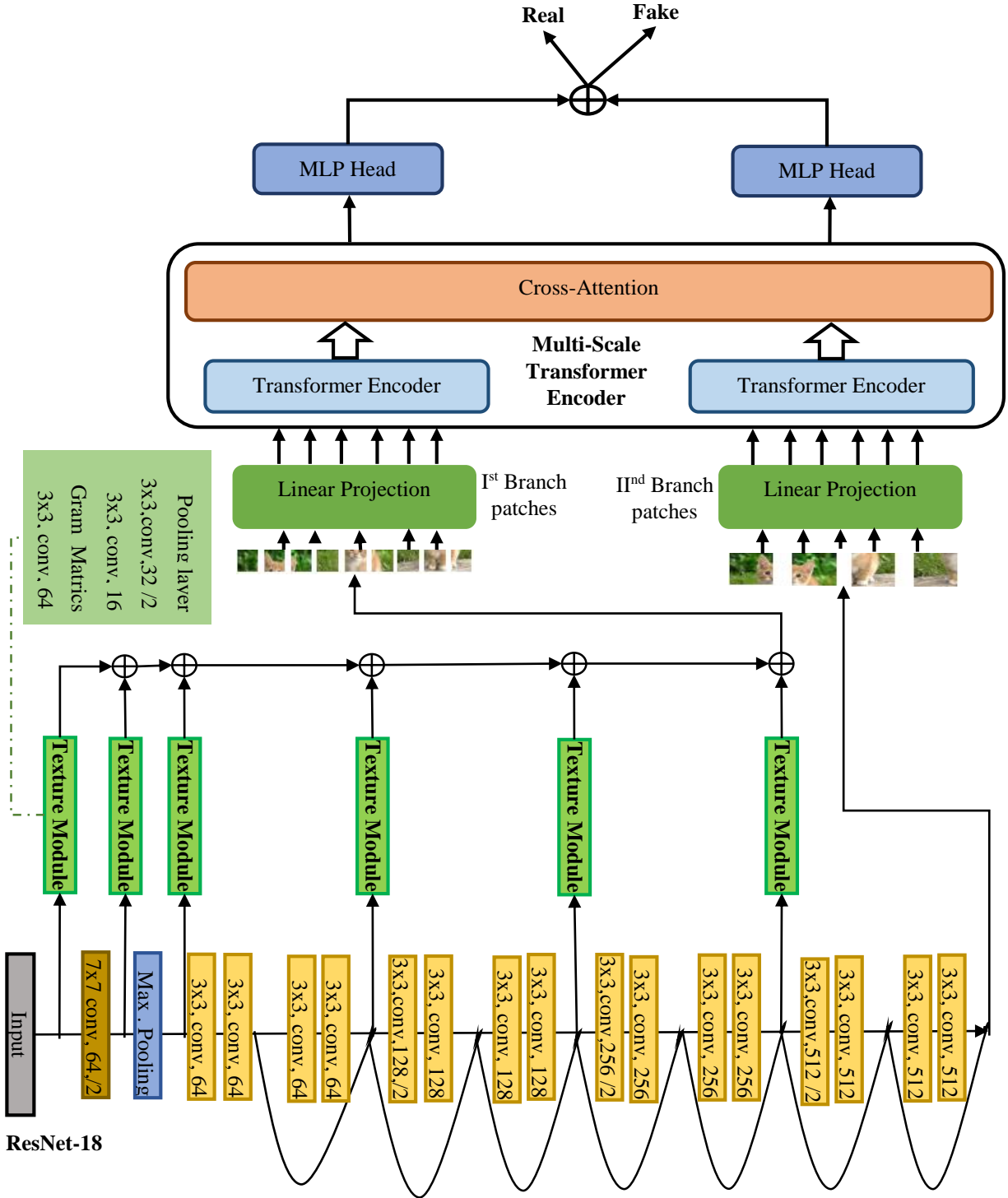


Figure 4: Proposed model consisting of texture module and ResNet serving as an input to dual-branch vision transformer with cross-attention mechanism

## 5 Experiments

This section will detail the choice of training hyperparameters, different datasets, the choice of face extractor, and the different experiment scenarios conducted.

### 5.1 Experimental Settings

The starting learning rate is set to 0.01. Adam optimizer is used to update the model's parameters, as it is being widely used and took less time for parameter updation in my case.

The batch size is taken as 64, due to the memory constraints at my computer systems. Each experiment is run for 100 epochs, as the model performance hits the saturation point after this specific number of epochs. The experiments are run for 24GB NVIDIA TITAN RTX GPUs.

## 5.2 Dataset Pre-Processing

Three deepfake datasets are used to evaluate the models: Celeb-DF, DFDC-Preview, and Faceforensics++, as these are being widely used and also the state-of-the-art dataset in the current scenarios. These datasets consist of short facial videos from which the frames are extracted utilizing the RetinaFaceResNet50 face extractor, as the RetinaFaceResNet50 face extractor has a lesser failure rate than MTCNN. One hundred frames are extracted from each video. For a DFDC and Celeb-DF dataset, most faces have aspect ratios of [1, 1.5] and heights between [151, 200] pixels. Lastly, an FF++ has a size of [151, 200] and an aspect ratio of [1,1.5]( Table 1). Different GAN images are also used to evaluate the model. Fake images: ProGAN and StyleGAN images and real image datasets: CelebA-HQ, CelebA, and FFHQ are downloaded from their respective repositories. StarGAN and STGAN images are generated by executing the code from their GitHub repositories.

Table 1: Details for the training, validation, and testing dataset with their resolutions

Dataset	Training Set	Validation set	Testing set	Image Resolution
FF++(DeepFakes)	8000 authentic, 8000 manipulated image frames.	2000 authentic, 2000 manipulated image frames.	2000 authentic, 2000 manipulated image frames.	128x128
FF++(face2face)	8000 authentic, 8000 manipulated image frames.	2000 authentic, 2000 manipulated image frames.	2000 authentic, 2000 manipulated image frames.	128x128
FF++(Faceswap)	8000 authentic, 8000 manipulated image frames.	2000 authentic, 2000 manipulated image frames.	2000 authentic, 2000 manipulated image frames.	128x128
FF++(Neural Texture)	8000 authentic, 8000 manipulated image frames.	2000 authentic, 2000 manipulated image frames.	2000 authentic, 2000 manipulated image frames.	128x128
DFDCPreview	10,000 authentic, 8000 manipulated image frames.	1500 real, 1500 fake image frames.	1500 real, 1500 fake image frames.	128x128
Celeb-DF	10,000 authentic, 10,000 manipulated image frames.	8000 authentic, 8000 manipulated image frames.	8000 authentic, 8000 manipulated image frames.	128x128
CelebA-HQ & ProGAN	10,000(CelebA-HQ) & 10,000(ProGAN)	1500(CelebA-HQ) & 1500(ProGAN)	1500(CelebA-HQ) & 1500(ProGAN)	1024x1024
CelebA-HQ& StyleGAN	10,000(CelebA-HQ) & 10,000(StyleGAN)	1500(CelebA-HQ) & 1500(StyleGAN)	1500(CelebA-HQ) & 1500(StyleGAN)	1024x1024
FFHQ and StyleGAN	10,000(FFHQ) & 10,000(StyleGAN)	1500(FFHQ) & 1500(StyleGAN)	1500(FFHQ) & 1500(StyleGAN)	1024x1024
CelebA & StarGAN	10,000(CelebA) & 10,000(StarGAN)	1500(CelebA) & 1500(StarGAN)	1500(CelebA) & 1500(StarGAN)	128x128
CelebA & STGAN	10,000(CelebA) & 10,000(StarGAN)	1500(CelebA) & 1500(StarGAN)	1500(CelebA) & 1500(StarGAN)	128x128

## 5.3 Data Augmentation and Scaling

Usually, a vision transformer needs data for training to perform at par with the CNN model, as shown by the original ViT model [52]. However, with the rich set of careful data-augmentation techniques, DeiT [53] has shown promising results with fewer data and comparable

performance with the CNN model. For the proposed model, various data-augmentation techniques have been used, which include rand augmentation [54], cut mix [55], and mixup [56], along with the random-erasing [57] and drop path regularisation model techniques to improve the overall results of the classifications.

#### 5.4 Experiments on the cross-domain settings for the Faceforensics++ dataset

Experimentation has been performed on the various categories of Faceforensics++ [22]. The model is trained on one class of FF++ and tested on the same as on other varieties of FF++. Weights of the models that perform well on the validation are saved for evaluation on the test dataset. Even though a lot of state-of-the-art models have been introduced recently, it is still difficult to compare them fairly. This is partially because there is a dearth of publicly available codes for the models and training procedures that are unavailable to the research community. Consequently, we advocate for the community to embrace open-source software and for the generation strategies of large-scale datasets to be evaluated independently of the model's success. These kinds of actions are essential to maintaining equity and encouraging further developments in this area. For the comparison, four models are taken into consideration:

- a) MesoInception-4 model [58].
- b) Capsule Network [59].
- c) Combining Vision Transformers and Efficient Net(E-ViT) [60].
- d) UCF [36].
- e) IID [61].
- f) SIA[21]
- g) UIA[22]

Code for these models has been taken from their GitHub repository and customized according to the dataset, and more evaluation metrics have been added for comprehensive evaluation. These models have been trained on one category of manipulation and tested on other categories of manipulation of FF++. These experiments are necessary to test the performance of the models against various manipulations, which is necessary to validate the detector's generalization abilities.

Table 2 represents the score of the various models when trained on the DeepFakes category and tested on the various categories of the FF++. Various models score very well for the same type of manipulation, and few even score perfectly, or it can be said that they are overfitting. These overfitted models' performance degraded heavily when asked to classify other categories of FF++. MesoNet and CapsuleNet, which are considered the most advanced models for detecting forgery, get an accuracy score of approximately 50% when it comes to identifying manipulated images in the FF++ dataset. This is due to their limited ability to learn just traditional features from convolutional neural networks (CNN), which is insufficient for effectively detecting cross-manipulation scenarios. Among the latest techniques, the Uia and Ucf approaches, which are renowned for identifying shared characteristics among different types of manipulation, do not meet the necessary criteria for an effective deepfake detector that can be applied universally. Our model outperforms the other models, with an accuracy of 72%, specifically for the DF category of the dataset. The majority of models struggle to accurately categorize the face-swap category in FF++, and a small number of models performed below 50% accuracy. Our model's performance demonstrates that texture is a consistent characteristic that remains present across different types of facial alterations.

Table 3 represents the scores for the models trained on the face2face categories and tested on the other categories of the FF++ dataset. Once again, the different models excessively suit the face2face category, and their effectiveness significantly declines when applied to other

categories of manipulation. The CapsuleNet approach exhibits the poorest performance among all methods for cross-manipulation. When trained on the face2face category, all models perform significantly better than in the previous scenarios in cross-manipulation settings. This is likely because face2face involves facial re-enactment techniques that use video frames to create a highly detailed reconstruction of the face, taking into account different lighting conditions and facial emotions. These inherent characteristics enable the models to learn the implicit features of the manipulation, which in turn aids in cross-manipulation scenarios. Uia is a highly effective model with an accuracy score of approximately 70%. This model utilizes an unsupervised technique and incorporates an inconsistency-aware module to detect discrepancies among the patch-level data. The Sia approach has poor performance due to its heavy reliance on the attention mechanism, which can occasionally miss tiny abnormalities in the manipulations. Furthermore, several models exhibited subpar performance without any notable improvements.

Conversely, Tex-ViT maintains the general characteristics, avoids overfitting when the training and testing data are from the same distribution, and generalizes well to alternative distribution categories. The manipulation achieved scores of 73% and 71% for the DF and NT categories, respectively. The FS category score for the manipulation has increased compared to the score in the preceding table.

Table 4 represents the performance of the model when trained in the FS category and tested on additional variations of FF++. All of the models exhibit overfitting for the same category and demonstrate inadequate performance for the other manipulation categories. This is mostly attributed to the Faceswap construction technique, which utilizes facial landmark points to generate a 3D template. This template is then projected onto the target shape in order to minimize the disparity between the projected shape and the landmark points. The meticulous process, which involves precise shape mixing and color correction, poses a greater challenge for the detector to identify accurately. The Ucf and Uia model exhibits poor performance, with an accuracy score of approximately 50% when trained on the face swap manipulation. This highlights the fragility of the model under different circumstances. Sia has poor performance, although IID demonstrates slightly higher performance compared to previous models. This improvement can be attributed to the model's capability to learn both implicit and explicit characteristics. However, the overall performance still falls well short of the desired score. MesoNet and CapsuleNet exhibit substandard performance; however, the transformer-based model E-ViT demonstrates significantly superior performance owing to its hybrid model structure, which combines CNN and ViT to capture long-range dependencies. Our model encounters difficulty in accurately identifying this category of manipulation, with an accuracy score ranging from 62-67%. This is because the face swap-generating mechanism incorporates intricate generation techniques that our model finds challenging to detect.

Table 5 represents the final category of manipulation, wherein the model is trained using the NT category of manipulation and subsequently tested on the remaining categories. The models trained in this specific category of manipulation exhibit a commendable level of performance when compared to other categories of manipulation. The NT generation mechanism utilizes the texturing technique to understand the inherent characteristics of the data sample, enabling it to excel in the categories of manipulation. All the models exhibit comparable performance when trained on the NT category of manipulation, indicating that texture is one of the invariant properties that assist in their ability to perform in diverse types of manipulation. The majority of the models achieved a score above 70% when tested on the DF category of manipulation. With the exception of Ucf and IID, all models in the face2face

category perform well and even outperform the former category. However, the manipulation category (FS) consistently shows poor performance. Furthermore, the issue of overfitting persists in the NT category. Once again, our model outperforms the other models. The state-of-the-art (SoTA) model achieves an accuracy score of 77% in face-to-face manipulation and 76% in Deepfake manipulation categories, demonstrating higher performance compared to other models.

So, other models score almost perfectly when training and testing come from the same distribution but fail to generalize well for other distributions. In contrast, based on the texture module and cross-attention mechanism, our model performs well in almost various manipulations, effectively proving that texture is a potential feature that persists among different manipulations. However, every performance suffers from the FS category of manipulation of FF++. Figure 5 represents the ROC curves of various models for images trained on face2face and testing on different types.

### 5.5 Experiments on the cross-domain settings for GAN dataset images

Extensive testing has been done on various GAN-generated images. Complete image synthesis, such as StyleGAN, ProGAN, and Attribute manipulation images of StarGAN and STGAN, has been considered for analysis. High-resolution authentic images are taken from the FFHQ, CelebA-HQ, while low-resolution images are taken from the CelebA. Five real and fake image datasets have been designed for the fair and comprehensive evaluation: CelebA-HQ ProGAN, CelebA-HQ StyleGAN, FFHQ StyleGAN, CelebA StarGAN, and CelebA STGAN. To compare the results of these datasets, four state-of-the-art models have been considered:

- a) Xception with depth-wise separable convolution(Xception-Net) [62].
- b) CNN's generated images are easy to spot now(CNN-Net) [63].
- c) Efficient-Net [64].
- d) UCF [36].
- e) IID [61].
- f) SIA[21]
- g) UIA[22]

Once again, code has been extracted from the GitHub source and tailored to suit the dataset used for these models. Additionally, additional evaluation criteria have been incorporated to facilitate comparison evaluation. The model exhibits exceptional performance and surpasses the scores achieved by several state-of-the-art methodologies. Similarly, when it comes to FF++ models designed for cross-forgery, their current level of performance is still rather distant from the optimal score required for their practical implementation in real-world situations. Table 6 represents the score of these models on various datasets. It is evident that the scores of different models vary between datasets; they excel in one dataset but do poorly in another. It is evident that when the testing dataset contains both fake and actual images, models can promptly recognize them due to their training on these types of images, but they face difficulty in identifying the other class. For instance, in the initial row, a model that was trained on CelebA-HQ ProGAN and tested on CelebA-HQ StyleGAN, most models can accurately recognize the CelebA-HQ category, as indicated by the precision value. However, they struggle to correctly classify the other category, as indicated by their recall value. ProGAN and StyleGAN employ distinct modification techniques, leading to disparate feature spaces.

Consequently, models trained in one category exhibit suboptimal performance on the other. There is a noticeable similarity between the CelebA-HQ and FFHQ real datasets in terms of their characteristics, as a model trained on one dataset can achieve good performance on the other. For instance, a model that has been trained using the CelebAHQ StyleGAN has strong

performance when combined with the FFHQ StyleGAN. Among these scenarios, the IID model has performed exceptionally well. This is because the datasets used are completely synthetic, and the IID model is particularly adept at identifying implicit inconsistencies within the feature space. Tex-ViT consistently beats other models across a range of settings. The evidence indicates that the model acquires the typical distinguishing characteristics, including the overall texture that remains consistent despite different types of modification, whether it is generating a full image or altering various qualities. The recall metric score indicates that all the models struggle to identify the ProGAN images accurately. Remarkably, nearly all the models awarded a flawless rating to the photos that were trained using StarGAN and assessed using STGAN, and vice versa. This could potentially elucidate the rationale behind the utilization of comparable counterfeiting techniques in their production. . Figure 6 represents the ROC curves of various models for images trained and tested on different GAN image datasets.

### **5.6 Experiments on the in-domain settings for various post-processing operations of FF++, Celeb-DF, and DFDCPreview dataset**

One of the limitations of the different models is that they are not robust enough for various post-processing operations like blurring, compression, the addition of noise, scaling, translation, etc. [1]. To demonstrate the model's robustness, the primary post-processing operations on the test dataset are blurring, compression, and addition of noise. For blurring the images, Gaussian blur PyTorch transformation has been used with a kernel size of 7x7 and sigma 25; for the addition of noise, zero mean and standard deviation of 0.2 have been designed, and finally, for the compression, quality of the images has been degraded by 3x times(Figure 7). Models have been trained on the regular images but tested on the images undergoing various post-processing operations. Three primary deepfake datasets have been considered for evaluation. Again, four models have been used for the comparative assessment:

- a) MesoInception-4 model [58].
- b) Capsule Network [59].
- c) CNN's generated images are easy to spot now(CNN-Net) [63].
- d) UCF [36].
- e) IID [61].
- f) SIA[21]
- g) UIA[22]

*Testing dataset does not undergo any post-processing operations.* The first row of the table represents the results when the image has not undergone any processing operations; in that case, all the models have performed perfectly(Table 7). Without undergoing post-processing operations, every model in the FF++ dataset overfits and ultimately performs poorly for various post-processing activities. When comparing FF++ to DFDCPreview and Celeb-DF, FF++ models perform better. However, the score for the Celeb-DF dataset is lower, possibly because this dataset contains high-quality images that closely resemble genuine images, with constant lighting and texture, making it slightly more challenging. MesoNet has gotten the lowest amount compared to other competitive approaches, mostly due to its poor capacity to capture the traditional CNN features. The IID approach outperforms the other model, achieving a near-perfect score for the DFDCPreview dataset. The model's capacity to concentrate on the inconsistent characteristics connected to identity makes it particularly useful for face-swapping manipulations.

*Testing dataset undergoes blurring operations:* Here, the second row for each dataset represents the score for blurring operations. The performance has not degraded significantly

for the blurring operation, showing that the blurry images retain the manipulated artifacts of the non-blurry images. However, the images have been blurred to a significant extent. The performance of the models in the case of FF++ decreased by at least 12% when exposed to blur operations. For the DFDCPreview and Celeb-Df datasets, the performance showed a slight decline, around 3-6%, with a few exceptions for certain models. MesoNet exhibits a more pronounced decrease in performance for Celeb-DF and DFDCPreview because of their heavy reliance on traditional CNN capabilities. The IID model has seen a decline in performance, specifically for the FF++ dataset, but there is a slight reduction in performance for the other dataset. Sia and Uia exhibit superior resilience compared to other models when exposed to blurring operations. Other models are significantly impacted. Our model has improved its ability to withstand and recover from challenges, as indicated by a mere 1-2% decrease in performance for the DFDCPreview and Celeb-Df datasets. Moreover, almost 12% of the data samples continue to display discriminatory artifacts even after undergoing substantial blurring.

*Testing dataset undergoes compression:* The quality of the photographs was reduced by treble as a consequence of the compression. Compressing samples for the DFDCPreview and Celeb-DF datasets has a minimal effect on the models' performance, suggesting that the altered artifacts are not significantly affected by the reduction in size. The performance of models such as UCF, CNN-Net, Sia, and IID in the FF++ dataset has been significantly impacted, indicating that these models are not specifically designed for compression circumstances. Additionally, the dataset contains a variety of manipulations, which exacerbates the model's complication in comprehending the extensive distribution of features. The models' efficacy was minimally affected by the Celeb-DF dataset, while the DFDCPreview dataset had a slightly greater impact. Compression typically entails a reduction in the resolution of data sampling, which affects the smaller details and leads to distortions such as ringing, banding, blocking, and halo. The gradients in the smooth portions are significantly impaired by these distortions. Models that concentrate on specific artifacts encounter difficulties when confronted with a diverse array of intricate properties. Models that concentrate on a variety of artifacts at differing levels of detail are more likely to accurately classify intricate feature patterns. Our model prioritizes intricate attributes, commencing with the integration of conventional CNN features at multiple levels and texturing. It employs a cross-attention method to comprehend both global and local details by utilizing the capabilities of transformers. This enables the model to acquire nuanced, intricate characteristics at multiple levels with greater efficacy.

*Addition of Noise to the testing dataset:* The PyTorch transformation modifies the data samples with noise, which has a mean of zero and a standard deviation of 0.2. The results revealed a substantial decrease in the scores of all models, with IID, MesoNet CNN-Net, Sia, and Uia scoring as low as 50%. This underscores the susceptibility of these detection methods to the presence of noise. The IID model, which is intended to detect face-swap, has been significantly impacted by the introduction of noise in the FF++ and DFDC Preview datasets. This has resulted in erroneous classification and has rendered the model susceptible to adversarial perturbations. MesoNet is susceptible to a variety of adversarial strategies as a result of a significant decrease in its classification score. The quality of images is reduced by the presence of noise, which masks anomalies or inconsistencies and introduces random variations and patterns. Consequently, accurate or complete feature extraction is impeded. In order to achieve optimal performance on a noisy dataset, a model must either employ the attention mechanism to leverage multi-scale features that can effectively capture both local and global features that are resilient to noise, or employ sophisticated data augmentation techniques that introduce noise to aid in the model's classification learning. By utilizing the latter approach, our model

has been able to acquire intricate and resilient features that can withstand a variety of adversarial techniques. When the accuracy of the other model in the DFDCPreview dataset is less than 80%, the Tex\_ViT model consistently outperforms it with an accuracy score of 98%. Nevertheless, the model remains susceptible to the introduction of disturbance to a certain extent.

Table 2: Models trained on deepfake dataset of FF++ and tested on its different categories. Here, bold values represent the highest score among competitive methods.

Test	Ucf					IID					MesoNet					CapsuleNet					E-ViT					Sia					Uia					Tex-ViT(ours)				
	Pr	Re	F1	AUC	Acc	Pr	Re	F1	AUC	Acc	Pr	Re	F1	AUC	Acc	Pr	Re	F1	AUC	Acc	Pr	Re	F1	AUC	Acc	Pr	Re	F1	AUC	Acc	Pr	Re	F1	AUC	Acc	Pr	Re	F1	AUC	Acc
Df	0.9989	0.9985	0.9987	0.9987	0.9987	<b>1.0</b>	<b>1.0</b>	<b>1.0</b>	<b>1.0</b>	<b>1.0</b>	1.0	0.999	0.9994	1.0	0.9995	<b>1.0</b>	0.999	1.0	0.9995	1.0	0.9995	<b>1.0</b>	<b>1.0</b>	<b>1.0</b>	<b>1.0</b>	<b>1.0</b>	0.9829	0.982	0.9824	0.9985	0.9825									
F2F	0.791	0.263	0.263	0.697	0.6023	0.7790	0.2715	0.4026	0.7218	0.5972	0.6667	0.1455	0.2389	0.6345	0.5365	0.6239	0.151	0.2431	0.6159	0.53	0.755	0.165	0.2708	0.6479	0.5557	0.6464	0.3455	0.4503	0.6345	0.5783	0.7286	0.192	0.3039	0.6508	0.5602	<b>0.7242</b>	<b>0.6126</b>	<b>0.6637</b>	<b>0.7048</b>	<b>0.6948</b>
FS	0.224	0.018	0.033	0.711	0.5396	0.4637	0.016	0.0309	0.5621	0.4987	0.2168	0.0155	0.0289	0.2962	0.4797	0.3764	0.0335	0.0615	0.4207	0.489	0.392	0.265	0.4964	0.4700	0.4927	0.3245	0.0865	0.1365	0.3999	0.4532	0.4652	0.0435	0.0709	0.5062	0.4962 <sub>5</sub>	<b>0.6952</b>	<b>0.040</b>	<b>0.0756</b> <sub>4</sub>	<b>0.6547</b>	<b>0.6291</b>
NT	0.8164	0.238	0.368	0.6693	0.5923	0.8765	0.245	0.3829	0.7263	0.6025	0.7703	0.208	0.3275	0.6972	0.573	0.7132	0.25	0.3702	0.6639	0.5747	0.789	0.257	0.3877	0.6829	0.5942	0.6616	0.5025	0.5711	0.6707	0.6227	0.7794	0.304	0.4374	0.7097	0.609	<b>0.7248</b>	<b>0.6989</b>	<b>0.6541</b>	<b>0.7958</b>	<b>0.7028</b>

Table 3: Models trained on the face2face dataset of FF++ and tested on its different categories. Here, bold values represent the highest score among competitive methods.

Test	Ucf					IID					MesoNet					CapsuleNet					E-ViT					Sia					Uia					Tex-ViT(ours)				
	Pr	Re	F1	AUC	Acc	Pr	Re	F1	AUC	Acc	Pr	Re	F1	AUC	Acc	Pr	Re	F1	AUC	Acc	Pr	Re	F1	AUC	Acc	Pr	Re	F1	AUC	Acc	Pr	Re	F1	AUC	Acc	Pr	Re	F1	AUC	Acc
Df	0.8531	0.3165	0.4617	0.7533	0.631	0.8638	0.387	0.5345	0.8117	0.663	0.7459	0.367	0.4919	0.7085	0.621	0.8161	0.253	0.3862	0.6304	0.598	0.6751	0.2775	0.3933	0.6733	0.572	0.6217	0.544	0.5802	0.6560	0.6065	0.7305	0.6305	0.6768	0.777	0.6989	<b>0.7365</b>	<b>0.664</b>	<b>0.6983</b>	<b>0.7958</b>	<b>0.7133</b>
F2F	0.9975	0.9985	0.9980	0.9986	0.998	0.9995	1.0	0.9997	1.0	0.9997	<b>1.0</b>	0.9960	0.9995	0.9977	0.9999	0.9977	<b>1.0</b>	<b>1.0</b>	<b>1.0</b>	<b>1.0</b>	<b>1.0</b>	0.9714	0.9875	0.9794	0.9986	0.9793														
FS	0.644	0.124	0.2079	0.5282	0.5277	0.5780	0.1315	0.2143	0.6605	0.5177	0.5871	0.266	0.3662	0.6064	0.5395	0.6371	0.151	0.2441	0.566	0.5325	0.6399	0.2390	0.3480	0.5922	0.552	0.5676	0.5015	0.5325	0.6079	0.5597	0.7120	0.4315	0.5373	0.6473	0.6284	<b>0.6952</b>	<b>0.5982</b>	<b>0.6433</b>	<b>0.6987</b>	<b>0.6593</b>
NT	0.8092	0.314	0.4524	0.6827	0.62	0.7891	0.378	0.5111	0.7877	0.6384	0.6937	0.3375	0.4541	0.6843	0.5942	0.8122	0.2855	0.4224	0.6666	0.6097	0.7209	0.4855	0.5802	0.7106	0.649	0.6741	0.694	0.6839	0.7217	0.6792	0.7523	0.638	0.6904	0.7949	0.7139	<b>0.7604</b>	<b>0.689</b>	<b>0.7229</b>	<b>0.8152</b>	<b>0.7360</b>

Table 4: Models trained on the face swap dataset of FF++ and tested on its different categories. Here, bold values represent the highest score among competitive methods.

Test	Ucf					IID					MesoNet					CapsuleNet					E-ViT					Sia					Uia					Tex-ViT(ours)				
	Pr	Re	F1	AUC	Acc	Pr	Re	F1	AUC	Acc	Pr	Re	F1	AUC	Acc	Pr	Re	F1	AUC	Acc	Pr	Re	F1	AUC	Acc	Pr	Re	F1	AUC	Acc	Pr	Re	F1	AUC	Acc	Pr	Re	F1	AUC	Acc
Df	0.371	0.0305	0.0564	0.4577	0.4894	0.7414	0.3885	0.5098	0.7262	0.6226	0.5892	0.522	0.5535	0.6321	0.579	0.5375	0.0895	0.1534	0.5415	0.5065	0.6872	0.311	0.4282	0.6712	0.5847	0.6432	0.274	0.3843	0.6093	0.5610	0.5309	0.253	0.3427	0.5789	0.5147	<b>0.7746</b>	<b>0.2486</b>	<b>0.3764</b>	<b>0.6847</b>	<b>0.6248</b>
F2F	0.7403	0.1625	0.2665	0.5369	0.5527	<b>0.6943</b>	<b>0.4315</b>	<b>0.5322</b>	<b>0.6964</b>	<b>0.6207</b>	0.6216	0.5455	0.5811	0.6354	0.6067	0.6383	0.1985	0.3028	0.5568	0.5430	0.6700	0.3005	0.4149	0.573	0.5762	0.7391	0.35	0.4751	0.6554	0.6132	0.6722	0.4605	0.5465	0.6516	0.618	0.7546	0.2283	0.3505	0.6446	0.6078
FS	0.9969	0.9949	0.9949	0.9949	0.995	<b>1.0</b>	<b>1.0</b>	<b>1.0</b>	<b>1.0</b>	<b>1.0</b>	<b>1.0</b>	<b>1.0</b>	<b>1.0</b>	<b>1.0</b>	<b>1.0</b>	<b>1.0</b>	<b>1.0</b>	<b>1.0</b>	<b>1.0</b>	<b>1.0</b>	<b>1.0</b>	<b>1.0</b>	<b>1.0</b>	<b>1.0</b>	<b>1.0</b>	<b>1.0</b>	<b>1.0</b>	<b>1.0</b>	<b>1.0</b>	<b>1.0</b>	<b>1.0</b>	<b>1.0</b>	<b>1.0</b>	<b>1.0</b>	<b>1.0</b>	0.9853	0.9755	0.9804	0.9982	0.9805
NT	0.6137	0.058	0.105	0.4929	0.5107	0.6113	0.2855	0.3892	0.5926	0.552	0.5903	0.539	0.5635	0.6205	0.5825	0.5342	0.1365	0.2174	0.5350	0.5087	0.6246	0.2355	0.3420	0.5574	0.547	0.5770	0.219	0.3175	0.5467	0.5292	0.5275	0.2585	0.3469	0.5181	0.5135	<b>0.7589</b>	<b>0.6378</b>	<b>0.6931</b>	<b>0.7088</b>	<b>0.6728</b>

Table 5: Models trained on NTdataset of FF++ and tested on its different categories. Here, bold values represent the highest score among competitive methods.

Test	Ucf					IID					MesoNet					CapsuleNet					E-ViT					Sia					Uia					Tex-ViT(Ours)				
	Pr	Re	F1	AUC	Acc	Pr	Re	F1	AUC	Acc	Pr	Re	F1	AUC	Acc	Pr	Re	F1	AUC	Acc	Pr	Re	F1	AUC	Acc	Pr	Re	F1	AUC	Acc	Pr	Re	F1	AUC	Acc	Pr	Re	F1	AUC	Acc
Df	0.8814	0.613	0.7231	0.7860	0.7652	<b>0.7941</b>	<b>0.729</b>	<b>0.7601</b>	<b>0.8542</b>	<b>0.77</b>	0.7347	0.8145	0.7725	0.8287	0.7602	0.7619	0.616	0.6812	0.7801	0.7117	0.7894	0.6505	0.7133	0.8325	0.7385	0.7236	0.6335	0.6755	0.7699	0.6957	0.6966	0.6395	0.6668	0.7383	0.6805	0.7405	0.8045	0.7714	0.8394	0.7612
F2F	0.7989	0.379	0.5146	0.6384	0.642	0.7169	0.6245	0.6675	0.7843	0.6899	0.7276	0.8615	0.7889	0.8342	0.7695	0.7100	0.5045	0.5898	0.7265	0.6492	0.7583	0.739	0.7485	0.8374	0.7517	0.7369	0.7565	0.7466	0.8053	0.7432	0.7532	0.748	0.7506	0.8183	0.7514	<b>0.7672</b>	<b>0.7995</b>	<b>0.7830</b>	<b>0.8558</b>	<b>0.7785</b>
FS	0.2403	0.0465	0.078	0.4005	0.4497	0.3039	0.1295	0.1816	0.4045	0.4156	0.5013	0.3745	0.4287	0.5296	0.501	0.4557	0.1675	0.2449	0.4886	0.4837	0.4966	0.2235	0.3082	0.5057	0.4985	0.4798	0.304	0.3722	0.5189	0.4872	0.5543	0.429	0.4836	0.5606	0.542	<b>0.7072</b>	<b>0.5844</b>	<b>0.6399</b>	<b>0.8148</b>	<b>0.6408</b>
NT	0.9954	0.993	0.9945	0.9972	0.9945	0.9494	0.9955	0.9719	0.9999	0.9712	0.9985	1.0	0.9992	1.0	0.9992	1.0	0.9925	0.9959	0.9978	0.996	<b>1.0</b>	0.9645	0.9795	0.9719	0.9971	0.9718														

Table 6: Models trained and tested on the GAN datasets. Here, bold values represent the highest score among competitive methods.

Train	Test	Xception					Ucf					IID					CNN-Net					Efficient-Net					Sia					Uia					Tex-ViT(ours)								
		Pr.	Re.	F1	AUC	Acc.	Pr.	Re.	F1	AUC	Acc.	Pr.	Re.	F1	AUC	Acc.	Pr.	Re.	F1	AUC	Acc.	Pr.	Re.	F1	AUC	Acc.	Pr.	Re.	F1	AUC	Acc.	Pr.	Re.	F1	AUC	Acc.	Pr.	Re.	F1	AUC	Acc.				
CelebA-HQ_ProGAN	CelebAH_Q_StyleGAN	1.0	0.06	0.113	0.7899	0.53	0.9	0.006	0.0119	0.4645	0.50266	1.0	0.0033	0.0066	0.6842	0.50166	0.9714	0.1913	0.3212	0.9708	0.5957	1.0	0.008	0.0158	0.8466	0.504	1.0	0.165	0.2837	0.9378	0.5826	0.8	0.0053	0.0105	0.8654	0.502	0.8807	<b>0.64</b>	<b>0.7413</b>	<b>0.8925</b>	<b>0.7767</b>				
	FFHQ_StyleGAN	0.904	0.0506	0.0959	0.7546	0.5226	0.652	0.997	0.7884	0.7777	0.7169	0.8	0.0026	0.0053	0.6048	0.501	0.6098	0.3466	0.4465	0.6533	0.5703	0.7215	0.038	0.0721	0.7205	0.5116	0.7785	0.1546	0.2581	0.7254	0.5553	0.9666	0.0193	0.0379	0.7285	0.5093	<b>0.7695</b>	<b>0.6386</b>	<b>0.6980</b>	<b>0.8091</b>	<b>0.7237</b>				
CelebA-HQ_StyleGAN	CelebAH_Q_ProGAN	1.0	0.024	0.0468	0.6872	51.2	0.471	0.005	0.0105	0.4161	0.4966	0.5	0.5	0.5	0.5468	0.5	0.7889	0.0033	0.0066	0.8363	0.5013	1.0	0.006	0.0013	0.8093	0.5033	1.0	0.0053	0.0106	0.8450	0.5026	0.5	0.5	0.5	0.4708	0.5	<b>0.7134</b>	<b>0.5445</b>	<b>0.6176</b>	<b>0.6818</b>	<b>0.6065</b>				
	FFHQ_StyleGAN	0.8625	1.0	0.9262	0.9886	0.9203	0.732	0.999	0.8452	0.7735	0.8169	0.8631	<b>1.0</b>	<b>0.9265</b>	<b>0.9998</b>	<b>0.9206</b>	0.9931	0.9986	0.8619	0.9943	0.84	0.7420	0.9993	0.8517	0.9972	0.8260	0.6105	1.0	0.7581	0.9783	0.6810	0.7022	1.0	0.8251	0.9965	0.788	0.8409	0.948	0.8912	0.945	0.8843				
FFHQ_StyleGAN	CelebAH_Q_ProGAN	0.9806	0.2366	0.3813	0.8118	0.616	0.5	0.5	0.5	0.5	0.5	0.6666	0.0013	0.0026	0.6027	0.5033	0.7727	0.012	0.023	0.7799	0.506	0.9032	0.0186	0.0365	0.7952	0.5083	0.6363	0.0046	0.0092	0.5773	0.501	0.9643	0.036	0.0694	0.7862	0.51733	0.8421	<b>0.3626</b>	<b>0.506</b>	<b>0.7454</b>	<b>0.6473</b>				
	CelebAH_Q_StyleGAN	0.9946	0.9993	0.9970	0.9998	0.9970	0.996	0.99	0.9933	0.9979	0.9933	1.0	<b>0.9993</b>	<b>0.9996</b>	<b>0.9999</b>	<b>0.9996</b>	0.9998	0.9963	0.9963	0.9999	0.9963	0.9963	0.9993	0.9993	0.9993	0.9999	0.9993	0.9986	0.9973	0.9979	0.9999	0.998	0.998	0.9993	0.9983	0.9819	0.9793	0.9806	0.9968	0.9807					
CelebA StarGAN	CelebA STGAN	0.9993	1.0	0.9996	1.0	0.9996	0.999	1.0	0.9996	1.0	0.9996	1.0	1.0	1.0	1.0	1.0	1.0	1.0	1.0	1.0	1.0	1.0	1.0	1.0	1.0	1.0	1.0	1.0	1.0	1.0	1.0	1.0	1.0	1.0	1.0	1.0	1.0	1.0	0.9775	0.927	0.9517	0.9882	0.9530		
CelebA StarGAN	CelebA STGAN	0.9986	1.0	0.9993	0.9999	0.9993	1	1	1	1	1	1.0	1.0	1.0	1.0	1.0	1.0	1.0	1.0	1.0	1.0	1.0	1.0	1.0	1.0	1.0	1.0	1.0	1.0	1.0	1.0	1.0	1.0	1.0	1.0	1.0	1.0	1.0	1.0	1.0	0.9958	0.9493	0.9720	0.9961	0.9727

Table 7: Models trained on various datasets and tested under various conditions. Here, bold values represent the highest score among competitive methods.

Training Dataset	Testing Dataset	Ucf					IID					MesoNet					CapsuleNet					CNN-Net					Sia					Uia					Tex-ViT(ours)					
		Pr.	Re.	F1	AUC	Acc.	Pr.	Re.	F1	AUC	Acc.	Pr.	Re.	F1	AUC	Acc.	Pr.	Re.	F1	AUC	Acc.	Pr.	Re.	F1	AUC	Acc.	Pr.	Re.	F1	AUC	Acc.	Pr.	Re.	F1	AUC	Acc.	Pr.	Re.	F1	AUC	Acc.	
FF++	FF++	0.988	0.9915	0.9898	0.9968	0.9897	0.9897	0.9951	0.9923	0.9996	0.9923	0.8322	0.9998	0.9084	0.9968	0.8991	<b>0.9925</b>	<b>0.9993</b>	<b>0.9993</b>	<b>0.9997</b>	<b>0.9993</b>	0.9998	0.9996	0.9968	0.9999	0.9968	0.9973	0.9985	0.9979	0.9999	0.9979	0.9982	0.9992	0.9982	0.9986	0.9987	0.9368	0.9424	0.9396	0.9882	0.9395	
FF++	FF++ Blurry	0.673	0.9282	0.7803	0.8297	0.7386	0.575	0.9975	0.7299	0.8699	0.6304	0.5305	1.0	0.6933	0.9819	0.5575	0.628	0.9975	0.7715	0.8788	0.7039	0.9807	0.9982	0.8329	0.9831	0.7998	0.7540	0.958	0.8438	0.9336	0.8227	0.7151	1.0	0.8338	0.9854	0.8007	<b>0.7720</b>	<b>0.9894</b>	<b>0.8673</b>	<b>0.9644</b>	<b>0.8486</b>	
FF++	FF++ Noisy	0.642	0.6445	0.6433	0.6479	0.6415	0.5	0.5	0.5	0.5903	0.5	0.5235	0.9928	0.6854	0.7079	0.5445	0.6981	0.046	0.0092	0.5612	0.5013	0.5	0.5	0.5	0.5	0.5	0.5	0.0095	0.0186	0.4979	0.50	0.7489	0.1103	0.1923	0.6546	0.5366	<b>0.6425</b>	<b>0.7839</b>	<b>0.7061</b>	<b>0.7409</b>	<b>0.673</b>	
FF++	FF++ Compression	1.0	0.0025	0.0044	0.5784	0.5011	1.0	0.0094	0.0186	0.912	0.5047	<b>0.9262</b>	<b>0.9868</b>	<b>0.9555</b>	<b>0.9940</b>	<b>0.9541</b>	1.0	0.0032	0.0064	0.6939	0.5016	0.9376	0.0764	0.1419	0.9300	0.5381	0.9973	0.231	0.3751	0.9002	0.6151	0.9992	0.6947	0.8196	0.9914	0.8471	0.9713	0.8651	0.9159	0.9839	0.9206	
DFDCPre view	DFDCPre view	1.0	0.9996	0.9997	0.9997	0.9998	<b>1.0</b>	<b>1.0</b>	<b>1.0</b>	<b>1.0</b>	<b>1.0</b>	0.9900	0.9993	0.9947	0.9999	0.9946	1.0	0.9993	0.9996	0.9999	0.9996	0.9999	0.9986	0.9989	0.9999	0.9999	0.9999	1.0	0.9986	0.9993	1.0	0.9993	1.0	0.9993	0.9996	0.9999	0.9996	0.9926	0.9893	0.9909	0.9995	0.9910
DFDCPre view	DFDCPre view Blurry	0.998	0.7926	0.8838	0.9287	0.8956	1.0	0.8493	0.9185	0.9940	0.9246	0.9985	0.8913	0.9418	0.9981	0.945	1.0	0.748	0.8558	0.9881	0.874	0.9967	0.72	0.8372	0.9965	0.86	1.0	0.8273	0.9055	0.9957	0.9136	1.0	0.9433	0.9708	0.9999	0.9716	<b>0.9933</b>	<b>0.9893</b>	<b>0.9913</b>	<b>0.9992</b>	<b>0.9913</b>	
DFDCPre view	DFDCPre view Noisy	0.5	1.0	0.6666	0.5447	0.5	0.5	1.0	0.6666	0.50	0.5	0.5	1.0	0.6666	0.5	0.5	0.4999	0.9986	0.6662	0.7179	0.4996	0.5598	1.0	0.6666	0.6015	0.5	0.2727	0.01	0.019	0.4388	0.4916	0.4978	0.99	0.6625	0.6841	0.4956	<b>0.9788</b>	<b>0.986</b>	<b>0.9824</b>	<b>0.9985</b>	<b>0.982</b>	
DFDCPre view	DFDCPre view Compression	0.757	0.9999	0.8619	0.7940	0.84	0.9375	1.0	0.9677	0.9999	0.9666	0.9695	0.9986	0.9839	0.9834	0.5468	1.0	0.7070	0.9304	0.5856	0.9943	1.0	0.7587	0.9938	0.9939	0.9247	0.9986	0.9602	0.9989	0.9586	0.9621	0.9993	0.9803	0.9998	0.98	<b>0.9980</b>	<b>0.9986</b>	<b>0.9983</b>	<b>0.9999</b>	<b>0.9998</b>		
Celeb-DF	Celeb-DF	0.954	0.9543	0.9544	0.9605	0.9544	0.9227	0.9451	0.9338	0.9773	0.9330	0.8222	0.9075	0.8628	0.9259	0.8556	0.9418	0.9462	0.9441	0.9741	0.9439	0.9848	0.9376	0.9406	0.9814	0.9408	0.8483	0.9008	0.8738	0.9431	0.8698	0.9235	0.9298	0.9266	0.9823	0.9264	<b>0.976</b>	<b>0.9442</b>	<b>0.9603</b>	<b>0.9928</b>	<b>0.9610</b>	
Celeb-Df	Celeb-DF Blurry	0.830	0.9511	0.8865	0.8937	0.8782	0.7483	0.9397	0.8332	0.9174	0.8118	0.6291	0.9757	0.7649	0.8822	0.7002	0.8793	0.756	0.8130	0.8979	0.8261	0.9600	0.9421	0.8912	0.9574	0.885	0.8191	0.8792	0.8481	0.9189	0.8425	0.8717	0.9345	0.9020	0.9631	0.8985	<b>0.9502</b>	<b>0.9258</b>	<b>0.9379</b>	<b>0.9812</b>	<b>0.9387</b>	
Celeb-Df	Celeb-DF Noisy	0.5	1.0	0.6666	0.5083	0.50	0.6241	0.5	0.5	0.5427	0.50	0.5	0.5	0.5	0.5267	0.50	0.5	0.5	0.5	0.5696	0.5	0.5	0.5	0.5	0.513	0.50	0.4766	0.09312	0.15558	0.4947	0.4954	0.6924	0.1513	0.2484	0.6218	0.5421	<b>0.6649</b>	<b>0.7581</b>	<b>0.7084</b>	<b>0.7365</b>	<b>0.6721</b>	
Celeb-Df	Celeb-DF Compression	0.973	0.5248	0.6819	0.9124	0.7551	0.9048	0.7524	0.8216	0.9321	0.8366	0.9468	0.334	0.4938	0.9193	0.6576	0.9278	0.5146	0.6620	0.8951	0.7373	0.9344	0.534	0.6881	0.9328	0.758	0.7512	0.9086	0.8228	0.9093	0.8044	0.9192	0.778	0.8427	0.9481	0.8548	<b>0.9203</b>	<b>0.9252</b>	<b>0.9227</b>	<b>0.9793</b>	<b>0.9226</b>	

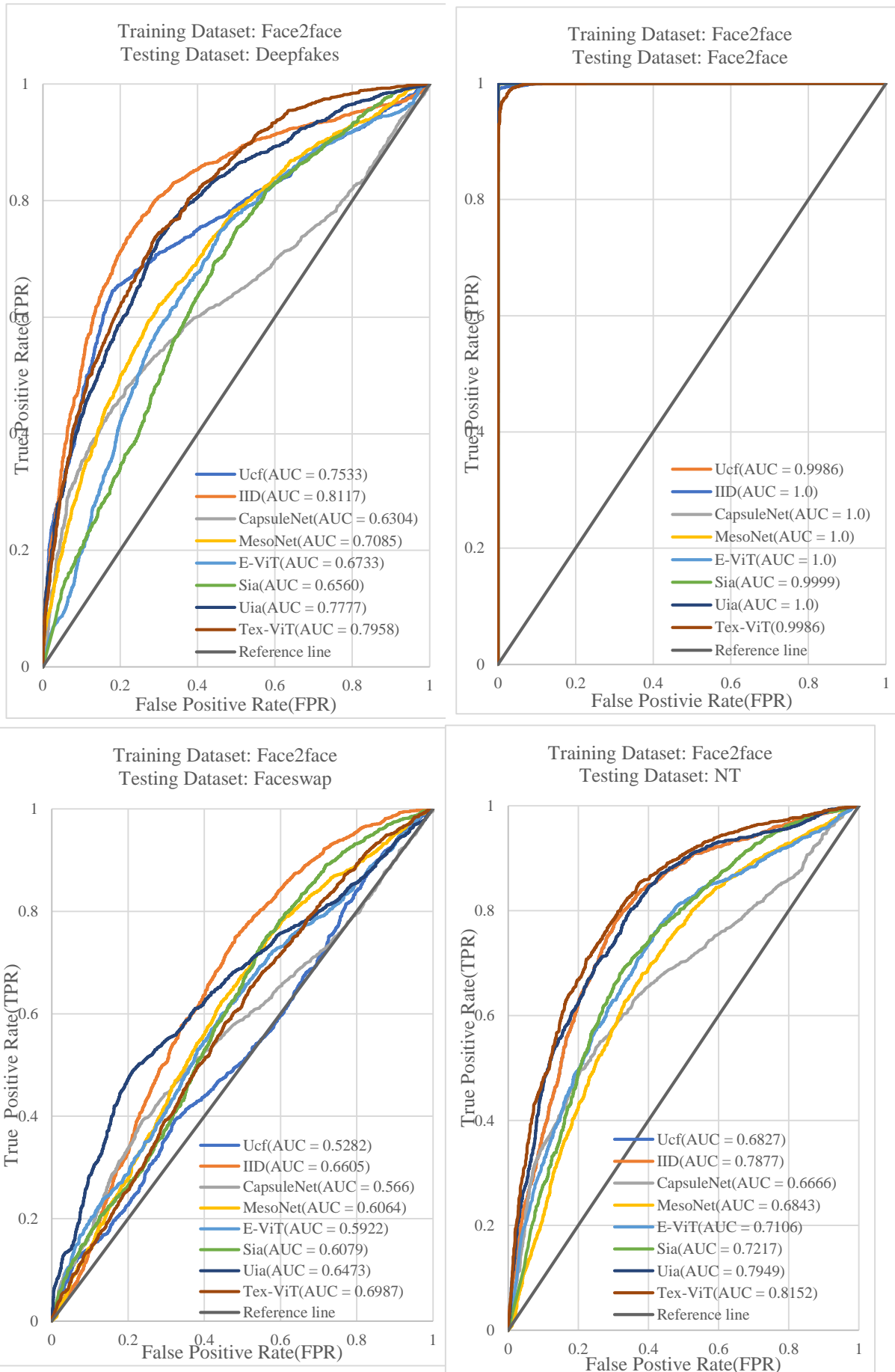


Figure 5: ROC curve for the model trained on Face2face dataset and tested on the other categories of FF++

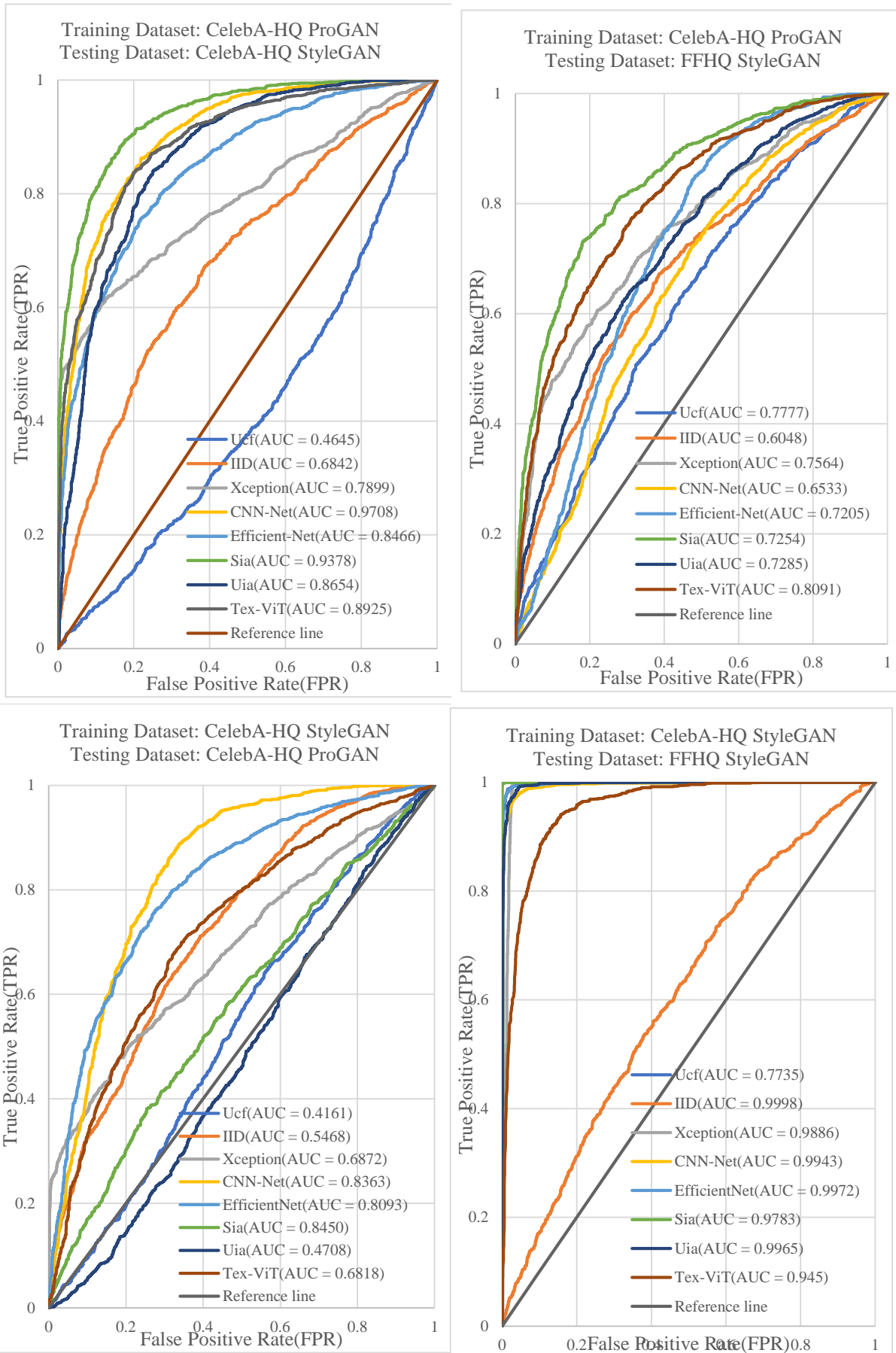


Figure 6: ROC curve for the model trained and tested on the different types of GAN images

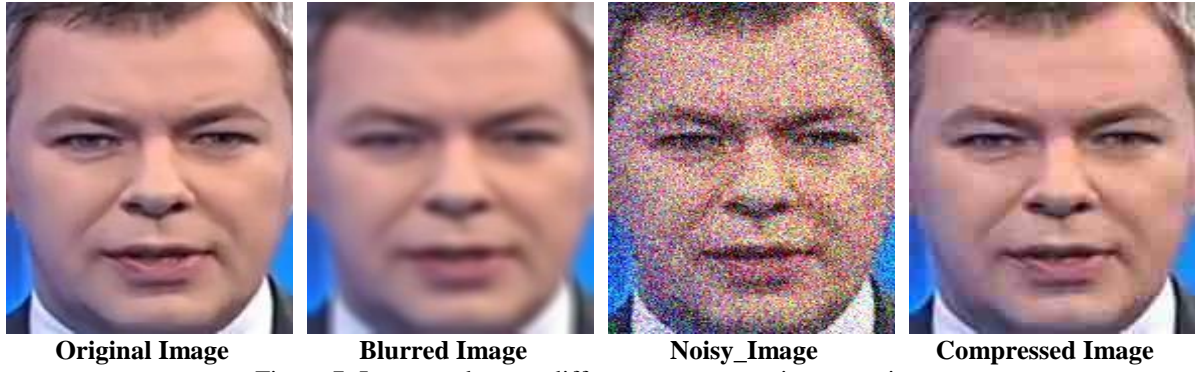


Figure 7: Image undergoes different post-processing operations

## 6 Ablation Studies

The ablation study is performed to confirm the validity of each Tex-ViT component, which is presented in this section. The experiments are performed on different categories of the Faceforensics++ dataset. The components are trained on three categories of FF++ and tested on the fourth category, and the process is done recursively for each category.

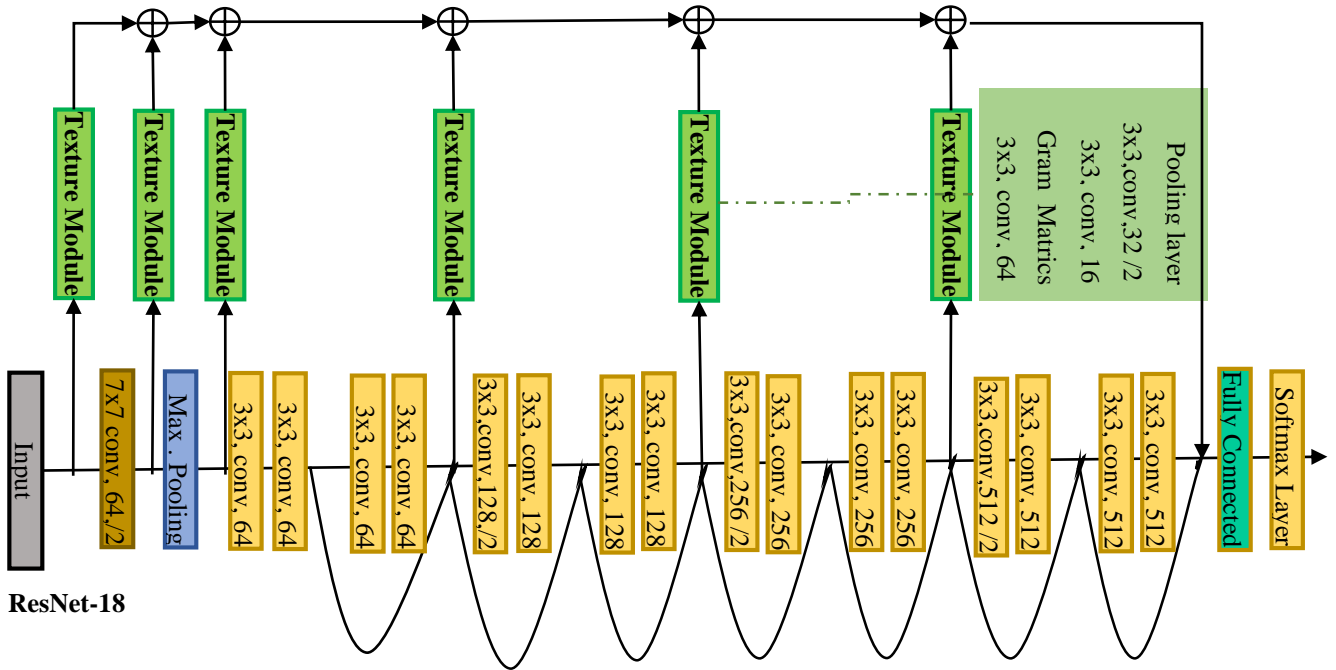


Figure 8: The ResNet18 model design includes a Texture block, in which the characteristics from both branches are combined using concatenation to make the final prediction.

### 6.1 ResNet with Texture module

This section features ResNet18 architecture as the backbone, and the texture block is computed before every downsampling operation. Furthermore, such texture features keep concatenating further and finally merging with the main branch. Finally, these concatenated features are passed fully connected and sigmoid layer for final prediction. Figure 8 shows the illustration of the component. Table 8 shows the classification results. The average accuracy score varies from 70 to 78%, showing that the texture, even without the attention mechanism, is a powerful feature representing the innate, inherent classification. Again, the component is struggling big-time for the face-swap category during classification, which can be understood as face-swap boundary inconsistencies that have a short range that may not be captured. The model can

effectively capture the discriminative features for other categories, showing that texture is impacted by the diverse manipulation method.

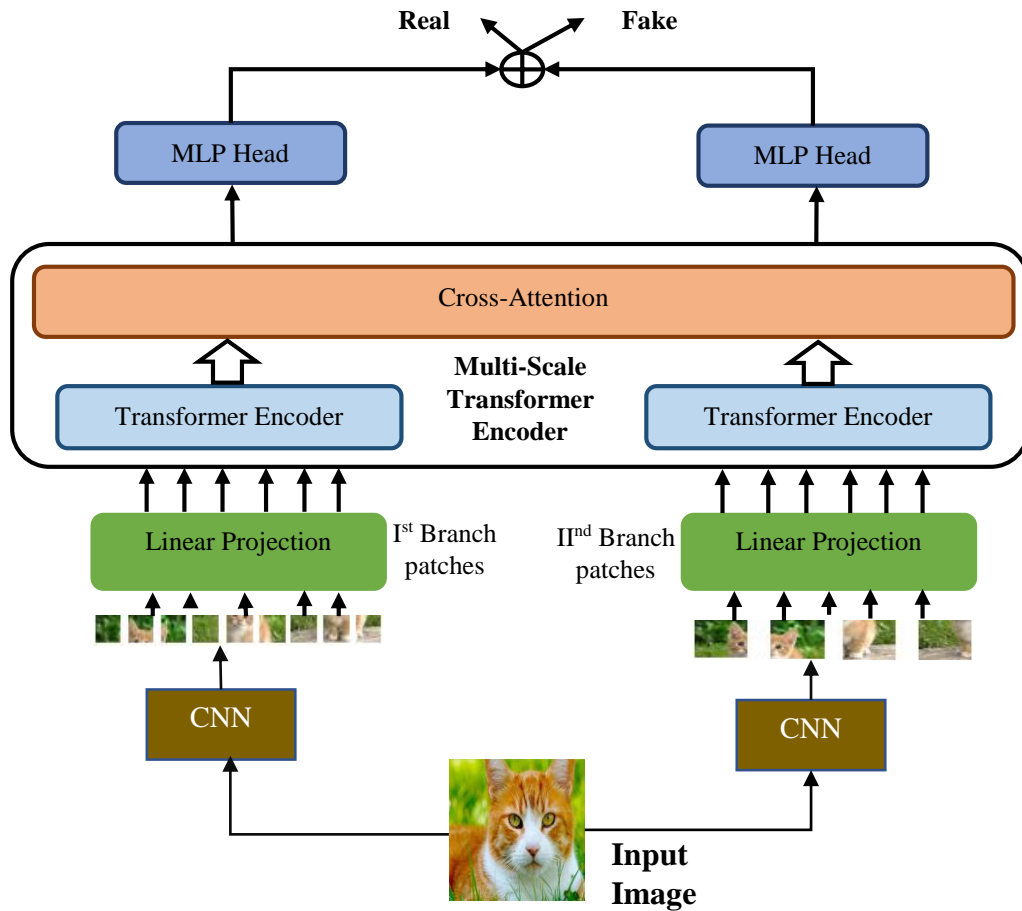


Figure 9: The Dual-branch cross-attention Vision transformer employs a model diagram in which the input image undergoes convolutional neural networks (CNNs) to generate feature maps of varying sizes.

## 6.2 Dual-branch cross-attention vision transformer

An illustration of this component is exhibited in Figure 9. Here, the input is passed through two CNNs at different branches, which produce feature maps of different sizes, which are subsequently passed to the transformer encoder for a cross-attention mechanism. Then, these features are passed to a multi-layer perceptron, and results are concatenated for final prediction. Table 8 shows the classification result of this component. Accuracy results range from 62 to 70%, which are below par compared to the former component, showing that conventional CNN features with cross-attention are insufficient to classify diverse manipulated images. For face swap samples, the score is more than the previous component, indicating that the attention mechanism has a significant role in places where texture features are not discriminative. The bottom line for this component is that a transformer with cross-attention is not enough to capture the significant latent inherent features that persist among various diverse manipulated samples.

## 6.3 Tex-ViT(ResNet+Texture Block + Cross-Attention Transformer)

Model, which is the combination of ResNet with texture block along with cross-attention transformer, has been proposed for this paper. As seen from the above component analysis,

texture could be a potential clue for deepfake detection that persists among various kinds of deepfake manipulation. At the same time, a cross-attention vision transformer, free of inductive biases, focuses on the specifics of the manipulation. The texture is computed and concatenated with conventional CNN features, and such features are further amplified, focussed, and augmented by the cross-attention mechanism, leading to a powerful feature representation and a better performance. The table clearly demonstrates that this potent combination results in an accuracy of eighty percent for Deepfake and Face2face samples, more than seventy for NT, and over sixty percent for face-swap. This confirms that the model is capable of acquiring distinguishing characteristics that are consistent across different types of samples.

Table 8 shows the classification results of the different components. Components are trained on different categories of FF++ and tested on the fourth category recursively, where Case A = F2F+FS+NT, Case B = DF+FS+NT, Case C = DF+F2F+NT, Case D= DF+F2F+FS

Train	Test	Precision	Recall	F1 Score	AUC	Acc
ResNet with Texture block						
Case A	DF	0.83	0.7045	0.7624	0.8784	0.78
Case B	F2F	0.882	0.7625	0.8179	0.9207	0.83
Case C	FS	0.4646	0.151	0.2279	0.5686	0.48
Case D	NT	0.7958	0.569	0.6635	0.8091	0.71
Dual-branch transformer augmented with Cross-Attention Mechanism						
Case A	DF	0.6578	0.7748	0.7115	0.7759	0.7001
Case B	F2F	0.6784	0.6956	0.6869	0.7489	0.6845
Case C	FS	0.6512	0.5512	0.5974	0.6748	0.6306
Case D	NT	0.7002	0.6785	0.68917	0.7458	0.6978
Tex-ViT (Our final model)						
Case A	DF	0.7901	0.949	0.8622	0.9275	0.8485
Case B	F2F	0.8364	0.8565	0.8463	0.9169	0.8463
Case C	FS	0.5773	0.543	0.5596	0.5900	0.57275
Case D	NT	0.7739	0.777	0.754	0.8600	0.775

Table 9 Tex-ViT's computational complexity is compared to well-known computer vision models. The column labeled "parameter" represents the number of trainable parameters. The accuracy score, number of trainable parameters, and GPU-CPU times taken for each input batch size are also included in the table.

Model	Accuracy	Parameter (millions)	CPU time(sec)	GPU time(sec)
CNN-Net	52.47	23.51	1.99s	0.379s
ResNext	79.55	81.41	4.61s	0.338s
CapsuleNet	60.56	1.5	2.49s	0.154
EfficientNetV2	80.5	118.51	3.93s	0.40s
XceptionNet	71.6	20.81	2.45s	0.66s
MesoInception	62.3	0.028	2.1s	0.72s
Swin Transformer	75.4	59.96	4.92s	0.41s
ResNet152	79.3	58	3.03s	0.309s
ConvNext	83.39	88.57	3.62	0.37s
Efficient_b7	75.49	66.34	4.07s	0.35s
<b>Tex-ViT</b>	<b>84.85</b>	<b>43</b>	<b>3.06s</b>	<b>1.02s</b>

## 7 Complexity Analysis of Tex-ViT

This section examines the computational complexity of the Tex-ViT architecture in comparison to established computer vision models. The computational factors to be taken into account are the quantity of trainable parameters, the level of precision achieved on the DF (FF++) dataset, and the inference times on both CPU and GPU.

Table 9 presents the tabular view of the complexity analysis of Tex-ViT against the various standard model of computer vision models. It can be easily seen that Tex-ViT is a reasonably light-weight model compared to various computer vision models, including EfficientNetv1, and has also achieved more excellent performance in diverse scenarios. Figure 10 represents the accuracy score on the y-axis and the number of trainable parameters on the x-axis. Regarding the number of trainable parameters, Efficientv2 and ConvNext are on the higher sides and have an accuracy score of around 80%; owning a higher number of parameters tends

to learn more discriminative information about the manipulation. Deepfake Detection models like MesoInceptionNet, Capsule Net, and CNN-Net are relatively light-weight, but their performance suffers in diverse scenarios. The execution time is measured in seconds for a batch size of 32 during inference time. Heavy models take more execution time than light-weight models due to their number of parameters. Xception is a light-weight model with 20 million parameters and an accuracy score of 70%.

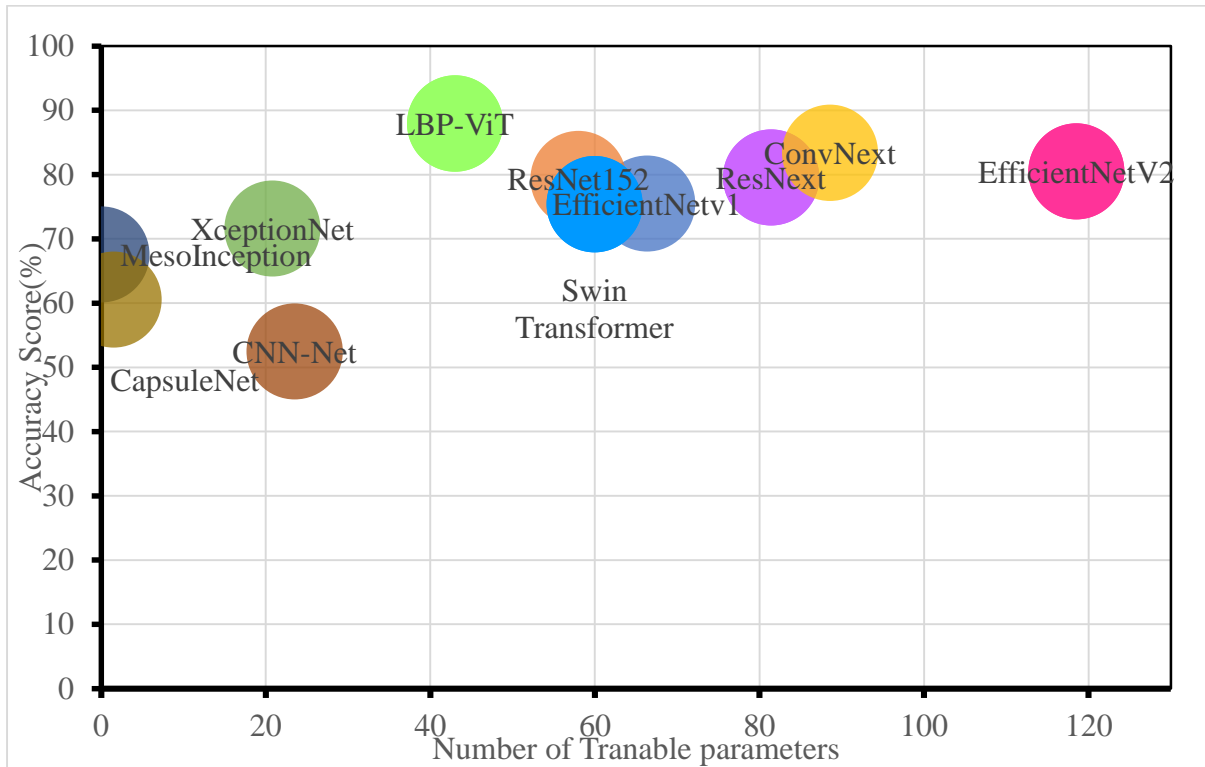


Figure 10 Tex-ViT's complexity analysis in comparison to well-known computer vision models.

### 8 Visualization results of the Tex-ViT's predictions

This section graphically shows the region of focus for the Tex-ViT prediction. Images are considered from every dataset, the model is trained, and then during prediction, GradCAM class activation maps are used to produce the region of focus for the classifier. Figure 11 shows the region of focus for the model's prediction. The model focuses on different regions of texture to produce the visualization results.





Figure 11: Tex-ViT's model's region of focus of feature for various datasets

## 9 Conclusion

In this paper, empirical analysis has been done on the human visual and CNN results to demonstrate that human vision is based on the shapes and CNN layers that use texture to identify objects. This finding indicates that texture is one crucial indicator for deepfake detection. Furthermore, it has been seen that texture correlation is not preserved in the case of fake images and that images tend to have smoother surfaces. Inspired by that, the proposed Tex-ViT uses the conventional CNN features using ResNet and texture modules using the features of ResNet. Then, the output of these two parallel branches serves as an input to the dual-branch vision transformers operating on patches with the cross-attention mechanism. Experimental results show that the model performs well in the cross-domain setting of FF++ datasets and different types of GAN image datasets and outperforms the other state-of-the-art models. Experimentation is done on various post-processing image scenarios, and it was found that the model is robust enough for different adversarial attacks. These experiments show that the model learns the common discriminative features that persist along several fake images. One limitation of the method is that it does not perform well in cross-domain settings when testing images from the faceswap category, and this could be future work, improving the model's accuracy on the Faceswap category of FF++. The evaluation shows that texture is an invariant feature that persists among various manipulation methods, and learning such a feature would eventually result in a good performance for the model. However, the model has a low score in the FS category of FF++. Experimentation is also done on the different types of GAN image datasets and outperforms the other state-of-the-art models. It again shows the model's superior learning abilities for different feature spaces. Experimentation is done on various post-processing image scenarios, and it was found that the model is robust enough for different adversarial operations. However, the model needs to improve its score for compressed scenarios, but its score is still better than the other SoTA models. These experiments show that the model learns the common discriminative features that persist along several fake images.

Future work would involve improving the model's accuracy for the FS manipulation category of FF++, which could incorporate additional modules to enhance the learning of features. Also, improving the model's robustness against the compressed data samples would be one of the futuristic works.

## 10 Author's contributions, compliance with Ethical standards, declaration of competing interests, availability and informed consent of data.

### *Author's contribution*

**Deepak Dagar:** Software, Validation, Investigation, Data Curation, Writing – Original Draft, Visualization.

**Dinesh Kumar Vishwakarma:** Conceptualization, Methodology, Formal Analysis, Resources, Writing – Review & Editing, Supervision, Project Administration, Funding Acquisition.

### *Compliance with Ethical Standards*

The authors affirm that the manuscript has adhered to the ethical standards specified by the Journal of Information Security and Applications.

### *Competing interests*

The authors affirm that they do not possess any identifiable conflicting financial or non-financial interests or personal ties that could have potentially influenced the findings presented in the research.

### *Research Data Policy and Data Availability Statements*

Given that the dataset and its corresponding code are open-source and accessible to the public. Therefore, it is unnecessary to acquire informed consent from the pertinent stakeholders before use the dataset.

## 11 References

- [1] D. Dagar and D. K. Vishwakarma, "A literature review and perspectives in deepfakes: generation, detection, and applications," *International Journal of Multimedia Information Retrieval*, vol. 11, pp. 219-289, 2022.
- [2] "All you need to know about deepfakes and why they are dangerous," [Online]. Available: <https://www.zee5.com/articles/all-you-need-to-know-about-deepfakes-and-why-they-are-dangerous>.
- [3] S. McCloskey and . M. Albright, "Detecting GAN-generated Imagery using Color Cues," in *arXiv:1812.08247v1*, 2018.
- [4] N. Yu, L. Davis and M. Fritz, "Attributing Fake Images to GANs: Learning and Analyzing GAN Fingerprints," in *IEEE/CVF International Conference on Computer Vision (ICCV)*, Seoul, 2019.
- [5] L. Li, J. Bao, T. Zhang, H. Yang, D. Chen, F. Wen and B. Guo, "Face X-ray for More General Face Forgery Detection," in *IEEE/CVF Conference on Computer Vision and Pattern Recognition (CVPR)*, Seattle, 2020.
- [6] F. Matern, C. Riess and M. Stamminger, "Exploiting Visual Artifacts to Expose Deepfakes and Face Manipulations," in *IEEE Winter Applications of Computer Vision Workshops (WACVW)*, Waikoloa, 2019.

- [7] X. Yang, Y. Li and S. Lyu, "Exposing Deep Fakes Using Inconsistent Head Poses," in *IEEE International Conference on Acoustics, Speech and Signal Processing (ICASSP)*, Brighton, 2019.
- [8] Y. Li, M.-C. Chang and S. Lyu, "In Ictu Oculi: Exposing AI Created Fake Videos by Detecting Eye Blinking," in *IEEE International Workshop on Information Forensics and Security (WIFS)*, Hong Kong, 2018.
- [9] D. Güera and E. J. Delp, "Deepfake Video Detection Using Recurrent Neural Networks," in *2018 15th IEEE International Conference on Advanced Video and Signal Based Surveillance (AVSS)*, Auckland, 2018.
- [10] I. Amerini, L. Galteri, R. Caldelli and A. D. Bimbo, "Deepfake Video Detection through Optical Flow based CNN," in *IEEE/CVF International Conference on Computer Vision Workshop (ICCVW)*, Seoul, 2019.
- [11] S. Agarwal, H. Farid, O. Fried and M. Agrawala, "Detecting Deep-Fake Videos from Phoneme-Viseme Mismatches," in *IEEE/CVF Conference on Computer Vision and Pattern Recognition Workshops (CVPRW)*, Seattle, 2020.
- [12] T. Mittal, U. Bhattacharya, R. Chandra, A. Bera and D. Manocha, "Emotions Don't Lie: An Audio-Visual Deepfake Detection Method using Affective Cues," in *ACM International Conference on Multimedia*, New York, 2020.
- [13] H. Khalid and S. S. Woo, "OC-FakeDect: Classifying Deepfakes Using One-class Variational Autoencoder," in *IEEE/CVF Conference on Computer Vision and Pattern Recognition Workshops*, Seattle, 2020.
- [14] X. Xuan, B. Peng, W. Wang and J. Dong, "On the Generalization of GAN Image Forensics," in *Chinese Conference on Biometric Recognition*, Zhuzhou, 2019.
- [15] F. Juefei-Xu, R. Wang, Y. Huang, Q. Guo, L. Ma and Y. Liu, "Countering Malicious DeepFakes: Survey, Battleground, and Horizon," in *arXiv:2103.00218v1*, 2021.
- [16] Z. Liu, X. Qi and H. S. P. Torr, "Global Texture Enhancement for Fake Face Detection In the Wild," in *Conference on Computer Vision and Pattern Recognition(CVPR)*, Virtual, 2020.
- [17] M. Bonomi, C. Pasquini and G. Boato, "Dynamic texture analysis for detecting fake faces in video sequences," *Journal of Visual Communication and Image Representation*, vol. 79, 2021.
- [18] J. Yang, S. Xiao, A. Li, . W. Lu, X. Gao and Y. Li, "MSTA-Net: Forgery Detection by Generating Manipulation Trace Based on Multi-scale Self-texture Attention," *IEEE TRANSACTIONS ON CIRCUITS AND SYSTEMS FOR VIDEO TECHNOLOGY*, vol. 32, no. 7, pp. 4854 - 4866, 2021.

- [19] I. Goodfellow, J. Pouget-Abadie, M. Mirza, B. Xu, D. Warde-Farley, S. Ozair, A. Courville and Y. Bengio, "Generative Adversarial Nets," in *Advances in Neural Information Processing Systems*, Montreal Canada, 2014.
- [20] "FaceSwap," [Online]. Available: <https://faceswap.dev/>. [Accessed August 2024].
- [21] "FakeApp," [Online]. Available: <https://www.malavida.com/en/soft/fakeapp/>. [Accessed August 2024].
- [22] A. Rössler, D. Cozzolino, L. Verdoliva, C. Riess, J. Thies and M. Niessner, "FaceForensics++: Learning to Detect Manipulated Facial Images," in *IEEE/CVF International Conference on Computer Vision (ICCV)*, Seoul, Korea, 2019.
- [23] L. Li, J. Bao, H. Yang, D. Chen and F. Wen, "Advancing High Fidelity Identity Swapping for Forgery Detection," in *IEEE/CVF Conference on Computer Vision and Pattern Recognition (CVPR)*, Washington, 2020.
- [24] Y. Choi, M. Choi, M. Kim, J.-W. Ha, S. Kim and J. Choo, "StarGAN: Unified Generative Adversarial Networks for Multi-domain Image-to-Image Translation," in *2018 IEEE/CVF Conference on Computer Vision and Pattern Recognition*, Salt Lake City, UT, USA, 2018.
- [25] M. Liu, Y. Ding, M. Xia, X. Liu, E. Ding, W. Zuo and S. Wen, "STGAN: A Unified Selective Transfer Network for Arbitrary Image Attribute Editing," in *IEEE/CVF Conference on Computer Vision and Pattern Recognition (CVPR)*, Long Beach, CA, USA, 2019.
- [26] R. Wang, F. Juefei-Xu, L. Ma, X. Xie, Y. Huang, J. Wang and Y. Liu, "FakeSpotter: A Simple yet Robust Baseline for Spotting AI-Synthesized Fake Faces," in *Proceedings of the Twenty-Ninth International Joint Conference on Artificial Intelligence*, 2020.
- [27] M. Barni, K. Kallas, E. Nowroozi and B. Tondi, "CNN Detection of GAN-Generated Face Images based on Cross-Band Co-occurrences Analysis," in *IEEE International Workshop on Information Forensics and Security (WIFS)*, New York, 2020.
- [28] L. Nataraj, T. M. Mohammed, S. Chandrasekaran, A. Flenner, J. H. Bappy, A. K. Roy-Chowdhury and B. S. Manjunath, "Detecting GAN generated Fake Images using Co-occurrence Matrices," 2019.
- [29] A. Jevnisek and S. Avidan, "Aggregating Layers for Deepfake Detection," in *International Conference on Pattern Recognition (ICPR)*, Montreal, QC, Canada, 2022.
- [30] Y. Lin, H. Chen, B. Li and J. Wu, "Towards Generalizable DEEPFAKE Face Forgery Detection with Semi-Supervised Learning and Knowledge Distillation," in *IEEE International Conference on Image Processing (ICIP)*, Bordeaux, France, 2022.
- [31] H. Chen, Y. Lin, B. Li and S. Tan, "Learning Features of Intra-Consistency and Inter-Diversity: Keys Toward Generalizable Deepfake Detection," *IEEE Transactions on Circuits and Systems for Video Technology*, vol. 33, no. 3, pp. 11468-1480, 2023.

- [32] Z. Hou, Z. Hua, K. Zhang and Y. Zhang, "CDNet: Cluster Decision for Deepfake Detection Generalization," in *IEEE International Conference on Image Processing (ICIP)*, Kuala Lumpur, Malaysia, 2023.
- [33] W. Guan, W. Wang, J. Dong and B. Peng, "Improving Generalization of Deepfake Detectors by Imposing Gradient Regularization," *IEEE Transactions on Information Forensics and Security*, vol. 19, 2024.
- [34] Z. Guo, L. Wang, W. Yang, G. Yang and K. Li, "LDFnet: Lightweight Dynamic Fusion Network for Face Forgery Detection by Integrating Local Artifacts and Global Texture Information," *IEEE Transactions on Circuits and Systems for Video Technology*, vol. 34, no. 2, pp. 1255 - 1265, 2024.
- [35] A. V. Nadimpalli and A. Rattani, "On Improving Cross-dataset Generalization of Deepfake Detectors," in *IEEE/CVF Conference on Computer Vision and Pattern Recognition Workshops (CVPRW)*, New Orleans, LA, USA, 2022.
- [36] Z. Yan, Y. Zhang, Y. Fan and B. Wu, "UCF: Uncovering Common Features for Generalizable Deepfake Detection," in *IEEE/CVF International Conference on Computer Vision (ICCV)*, Paris, France, 2023.
- [37] P. Yu, J. Fei, X. Zhihua, Z. Zhili and J. Weng, "Improving Generalization by Commonality Learning in Face Forgery Detection," *IEEE Transactions on Information Forensics and Security*, vol. 17, pp. 547-558, 2022.
- [38] M. Atamna, I. Tkachenko and S. Miguet, "Improving Generalization in Facial Manipulation Detection Using Image Noise Residuals and Temporal Features," in *IEEE International Conference on Image Processing (ICIP)*, Kuala Lumpur, Malaysia, 2023.
- [39] J. Li, Z. Yu, G. Luo and Y. Zhu, "CodeDetector: Revealing Forgery Traces with Codebook for Generalized Deepfake Detection," in *Proceedings of the 2024 International Conference on Multimedia Retrieval*, 2024.
- [40] J. Yang, S. Xiao, A. Li, G. Lan and H. Wang, "Detecting fake images by identifying potential texture difference," *Future Generation Computer Systems*, vol. 125, pp. 127-135, 2021.
- [41] J. Yang, A. Li, S. Xiao, W. Lu and X. Gao, "MTD-Net: Learning to Detect Deepfakes Images by Multi-Scale Texture Difference," *IEEE TRANSACTIONS ON INFORMATION FORENSICS AND SECURITY*, vol. 16, pp. 4234 - 4245, 2021.
- [42] A. Yadav and D. K. Vishwakarma, "MRT-Net: Auto-adaptive weighting of manipulation residuals and texture clues for face manipulation detection," *Expert Systems with Applications*, vol. 232, 2023.
- [43] J. Gao, M. Micheletto, G. Orrù, S. Concas, X. Feng, G. L. Marcialis and F. Roli, "Texture and artifact decomposition for improving generalization in deep-learning-based deepfake detection," *Engineering Application of Artificial Intelligence*, vol. 133, 2024.

- [44] J. Yang, S. Xiao, A. Li, . W. Lu, X. Gao and Y. Li, “MSTA-Net: Forgery Detection by Generating Manipulation Trace Based on Multi-scale Self-texture Attention,” *IEEE TRANSACTIONS ON CIRCUITS AND SYSTEMS FOR VIDEO TECHNOLOGY*, vol. 32, no. 7, pp. 4854 - 4866, 2022.
- [45] R. Geirhos, P. Rubisch, C. Michaelis, M. Bethge, F. A. Wichmann and W. Brendel, “ImageNet-trained CNNs are biased towards texture; increasing shape bias improves accuracy and robustness,” in *International Conference on Learning Representations (ICLR)*, New Orleans, 2019.
- [46] M. D. Zeiler and R. Fergus, “Visualizing and Understanding Convolutional Networks,” in *European Conference on Computer Vision*, Zurich, 2014.
- [47] H. Lee, R. Grosse, R. Ranganath and A. Y. Ng , “Convolutional deep belief networks for scalable unsupervised learning of hierarchical representations,” in *Proceedings of the 26th Annual International Conference on Machine Learning*, Montreal, 2009.
- [48] D. Dai, Y. Li, Y. Wang, H. Bao and G. Wang, “Rethinking the image feature biases exhibited by deep convolutional neural network models in image recognition,” *CAAI Transactions on Intelligence Technology*, vol. 7, no. 4, pp. 721-731, 2022.
- [49] W. Luo, Y. Li, R. Urtasun and R. Zemel, “Understanding the Effective Receptive Field in Deep Convolutional Neural Networks,” in *Proceedings of the 30th International Conference on Neural Information Processing Systems*, Barcelona, 2016.
- [50] L. A. Gatys, A. S. Ecker and M. Bethge, “Texture synthesis using convolutional neural networks,” in *Proceedings of the 28th International Conference on Neural Information Processing Systems*, Montreal, Quebec, Canada, 2015.
- [51] C.-F. (. Chen, Q. Fan and R. Panda, “CrossViT: Cross-Attention Multi-Scale Vision Transformer for Image Classification,” in *Computer Vision and Pattern Recognition*, Nashville, Tennessee, 2021.
- [52] A. Dosovitskiy, L. Beyer, A. Kolesnikov, D. Weissenborn, . X. Zhai, T. Unterthiner, M. Dehghani, M. Minderer, G. Heigold, S. Gelly, J. Uszkoreit and N. Houlsby, “An Image is Worth 16x16 Words: Transformers for Image Recognition at Scale,” in *2021, In International Conference on Learning Representations*.
- [53] H. Touvron, M. Cord, M. Douze, F. Massa, A. Sablayrolles and H. Jégou, “Training data-efficient image transformers & distillation through attention,” in *Proceedings of the 38th International Conference on Machine Learning*, 2021.
- [54] E. D. Cubuk, B. Zoph, J. Shlens and Q. V. Le, “RandAugment: Practical automated data augmentation with a reduced search space,” in *IEEE/CVF Conference on Computer Vision and Pattern Recognition Workshops (CVPRW)*, Seattle, WA, 2020.
- [55] S. Yun, D. Han, S. Chun, S. J. Oh, Y. Yoo and J. Choe, “CutMix: Regularization Strategy to Train Strong Classifiers With Localizable Features,” in *IEEE/CVF International Conference on Computer Vision (ICCV)*, Seoul, Korea, 2019.

- [56] H. Zhang, . M. Cisse, Y. N. Dauphin and D. Lopez-Paz, “mixup: Beyond Empirical Risk Minimization,” in *In International Conference on Learning Representations*, 2018.
- [57] Z. Zhong, L. Zheng, G. Kang, S. Li and Y. Yang, “Random Erasing Data Augmentation,” in *Proceedings of the AAAI Conference on Artificial Intelligence*,, 2020.
- [58] D. Afchar, V. Nozick, J. Yamagishi and I. Echizen, “MesoNet: a Compact Facial Video Forgery Detection Network,” in *IEEE International Workshop on Information Forensics and Security (WIFS)*, Hong Kong, China, 2019.
- [59] H. H. Nguyen, J. Yamagishi and I. Echizen, “Capsule-forensics: Using Capsule Networks to Detect Forged Images and Videos,” in *IEEE International Conference on Acoustics, Speech and Signal Processing (ICASSP)*, Brighton, UK, 2019.
- [60] D. Coccomini, . N. Messina, . C. Gennaro and F. Falchi, “Combining EfficientNet and Vision Transformers for Video Deepfake Detection,” in *International Conference on Image Analysis and Processing*, 2022.
- [61] B. Huang, Z. Wang, J. Yang, J. Ai, Q. Zou, Q. Wang and D. Ye, “Implicit Identity Driven Deepfake Face Swapping Detection,” in *IEEE/CVF Conference on Computer Vision and Pattern Recognition (CVPR)*, Vancouver, BC, Canada, 2023.
- [62] F. Chollet, “Xception: Deep Learning with Depth-wise Separable Convolutions,” in *IEEE Conference on Computer Vision and Pattern Recognition (CVPR)*, Honolulu, HI, USA, 2017.
- [63] S.-Y. Wang, O. Wang, R. Zhang, A. Owens and A. A. Efros, “CNN-Generated Images Are Surprisingly Easy to Spot... for Now,” in *IEEE/CVF Conference on Computer Vision and Pattern Recognition (CVPR)*, Seattle, WA, USA, 2020.
- [64] M. Tan and Q. V. Le, “EfficientNet: Rethinking Model Scaling for Convolutional Neural Networks,” in *International Conference on Machine Learning*, 2019.